TRENDS IN SCIENCES 2026; 23(8): 12566
https://doi.org/10.48048/tis.2026.12566
RESEARCH ARTICLE

Chemical Composition and Anti-Skin Cancer Potential of *Eucalyptus tereticornis* Essential Oils from Vietnam: An *In Vitro* and *In Silico* Study

Tran Hoang Ngau[1], Chau Dao Minh Huynh[2], Hoai Nguyen Thi Thanh[1], Ngan Pham Thu[1], Tran Ngo Bao Huynh[2], Thang Truong Le[3,4] and Viet Hoang[2,*]

[1]*Ho Chi Minh City University of Industry and Trade, Ho Chi Minh City 70000, Vietnam*
[2]*Faculty of Biology-Biotechnology, University of Science, VNUHCM, Ho Chi Minh City 70000, Vietnam*
[3]*Smart Medicine and Health Informatics Program, International College, National Taiwan University, Taipei 10617, Taiwan*
[4]*School of Medicine, College of Medicine, National Taiwan University, Taipei 10617, Taiwan*

([*]Corresponding author's e-mail: hviet@hcmus.edu.vn)

Received: 7 November 2025, Revised: 17 December 2025, Accepted: 24 December 2025, Published: 10 March 2026

Abstract

This study aimed to explore the therapeutic potential of *Eucalyptus tereticornis* essential oil in skin cancer treatment, with *E. camaldulensis* serving as a well-documented reference, both species collected in Vietnam. A multidisciplinary approach was employed to investigate chemical composition, cytotoxicity, anti-metastatic effects, and molecular mechanisms. The chemical constituents of the oils were characterized using gas chromatography-mass spectrometry (GC-MS). Cytotoxic effects were evaluated on murine melanoma B16F10 cells using the MTT assay. Anti-metastatic potential was investigated through cell migration (wound healing assay) and adhesion assays. To elucidate possible molecular mechanisms, molecular docking simulations were performed against key melanoma-related protein targets, including BRAF, NRAS, AKT3, FAK, and HDAC, and gene expression survival analysis stratified melanoma patient outcomes. GO and KEGG enrichment analyses were used to interpret functional roles. In cytotoxicity assays, *E. tereticornis* displayed a higher IC_{50} (152.9 µg/mL) compared to *E. camaldulensis* (182 µg/mL), suggesting higher anticancer efficacy. Moreover, *E. tereticornis* significantly inhibited B16F10 cell migration and adhesion, indicating potential anti-metastatic activity. GC-MS identified 46 compounds across both species. The dominant constituents in *E. tereticornis* were β-pinene, caryophyllene oxide, and α-pinene, while β-eudesmol, γ-terpinene, and o-cymene were major in *E. camaldulensis*. Docking results showed the strongest binding affinity to BRAF with the bicyclo[4.1.0]heptane, 7-bicyclo[4.1.0]hept-7-ylidene derivative (−8.5 kcal/mol). Survival analysis revealed significant prognostic associations for alloaromadendrene and caryophyllene-(I1) in melanoma patients ($p < 0.05$). *Eucalyptus* essential oils, particularly from *E. tereticornis*, exhibit promising antioxidant and anticancer activities, suggesting potential in melanoma therapy.

Keywords: *Eucalyptus tereticornis*, *Eucalyptus camaldulensis*, Anti-skin cancer, Molecular docking

Introduction

Skin cancer represents a major global health challenge and is one of the leading causes of dermatologic disease burden. Both melanoma and non-melanoma skin cancers contribute substantially to cancer incidence and mortality worldwide, particularly in regions with predominantly fair-skinned populations such as Australia, New Zealand, Europe, and North America [1]. In 2022 alone, an estimated 331,722 new cases of melanoma were reported globally, making it the 17th most common cancer and leading to approximately 58,667 deaths [2]. In the United States, projections for 2025 indicate 104,960 new invasive melanoma cases and 107,240 melanoma in situ cases, with about 8,430 deaths expected [3]. These statistics emphasize the

urgent need for new and effective preventive and therapeutic strategies against skin cancer.

In the search for novel anticancer agents, natural products have gained increasing attention due to their diverse bioactive compounds. Among these, the *Eucalyptus* genus stands out for its pharmacological potential [4]. With over 700 species, *Eucalyptus* is one of the most commonly cultivated genera in forest plantations worldwide. *Eucalyptus globulus* is the most widely planted species, followed by *E. camaldulensis*, *E. tereticornis*, *E. nitens*, and *E. saligna* [5]. *Eucalyptus* leaves and essential oils are known for their medicinal properties, including analgesic, anti-inflammatory, antioxidant, antimicrobial, and anticancer activities [4,6].

Of these species, *E. camaldulensis* has been extensively investigated and shown to possess cytotoxic effects against various cancer cell lines, including melanoma (B16F10), breast (MCF-7), lung (A549), colon (Caco-2), and liver (HepG2) cancers [7,8]. In addition, its extracts have demonstrated inhibitory effects on melanogenesis through modulation of MAPK and PKA signaling pathways [7]. By contrast, *E. tereticornis*, although widely cultivated and chemically rich, has received comparatively less attention, despite evidence of bioactivity against lung cancer cells [9]. This underexplored potential makes *E. tereticornis* a compelling candidate for further study, particularly in the context of skin cancer.

The therapeutic promise of *Eucalyptus* species largely derives from compounds such as 1,8-cineole, macrocarpals, eucalyptin, monoterpenes (p-cymene, α-pinene, and d-limonene), and various flavonoids and chalcones, which have been reported to inhibit cancer cell proliferation, induce apoptosis, and modulate oxidative stress pathways [4,8,10-12]. Collectively, these phytochemicals likely contribute to the anticancer activities of *Eucalyptus* essential oils through multiple complementary pathways, reinforcing the therapeutic promise of species such as *E. tereticornis* in cancer treatment-particularly in the context of skin cancer.

In Vietnam, *Eucalyptus camaldulensis* and *Eucalyptus tereticornis* are widely cultivated, especially in the central and southern regions, to supply wood for various industries and support reforestation initiatives [13]. However, their compound profile and potential applications in skin cancer are sufficiently studied and understood [14,15]. To address this gap, the present study conducts a comparative evaluation between the two species, using *E. camaldulensis* as a well-documented reference and highlighting the unexplored potential of *E. tereticornis*. An integrative approach was employed, combining chemical analysis, biological evaluation, and computational modeling. Essential oil constituents were identified using gas chromatography-mass spectrometry (GC-MS), followed by *in vitro* assays on B16F10 melanoma cells to assess cytotoxicity, cell migration, and adhesion inhibition. To predict molecular interactions, molecular docking was performed between major bioactive compounds and cancer-related protein targets [16]. Additionally, survival analysis of gene expression was conducted to stratify melanoma patients into high- and low-risk groups [17]. To elucidate the functional roles of the predicted targets, GO and KEGG pathway enrichment analyses were carried out, providing insights into the biological processes and signaling pathways potentially modulated by *Eucalyptus*-derived compounds in melanoma [18,19].

Overall, this study aims to bridge the knowledge gap by integrating chemical profiling, biological activity evaluation, and computational modeling of *E. tereticornis* essential oils. The findings are expected to illuminate their therapeutic potential and guide future research and development in the field of natural product-based drug discovery.

Materials and methods

Plant material and extractions

Plant samples collected in the Mekong Delta, Vietnam, were taxonomically verified by the Department of Ecology and Evolutionary Biology based on morphological characteristics. Voucher specimens of *Eucalyptus camaldulensis* (PHH1004930) and *Eucalyptus tereticornis* (PHH1004931) have been deposited at the PHH Herbarium, University of Sciences, VNU-HCM. Fresh leaves (10 kg) were distilled for three hours at 100 °C using a Clevenger apparatus. The resulting essential oil was dried with anhydrous sodium sulfate and stored at –20 °C. The extraction process was repeated three times, and the essential oil yield was averaged based on fresh plant

weight. For additional testing, the extracted oil was then combined with DMSO (dimethyl sulfoxide).

Cytotoxicity activity

B16F10 (murine melanoma) was provided by ATCC (American Type Culture Collection, Manassas, VA, USA). Cell viability of B16F10 cell lines exposed to the sample extract was evaluated using the MTT assay (3-(4,5-dimethylthiazol-2-yl)-2,5-diphenyltetrazolium) [20]. Cells (3×10^3 per well) were seeded in a 96-well plate and incubated overnight for adhesion [21]. The medium was then refreshed with 95 µL of fresh media, and cells were treated with extract concentrations ranging from 7.813 to 2,000 µg/mL, prepared by serial dilution. After 48 h of exposure, 5 mg/mL MTT solution was added to each well, followed by a 4-hour incubation. Formazan crystals were solubilized using 100 µL of 99.9% DMSO, and absorbance was measured at 540 nm. A positive control was doxorubicin with concentrations ranging from 0.03125 to 1 µg/mL.

Timepoint effect of IC_{50} of essential oils

Cell viability of B16F10 cell lines exposed to the sample extract was evaluated using the MTT assay (3-(4,5-dimethylthiazol-2-yl)-2,5-diphenyltetrazolium) [20,22]. Cells (3×10^3 per well) were seeded in a 96-well plate and incubated overnight for adhesion. The medium was then refreshed with 95 µL of fresh media, and cells were treated with extract concentrations of IC_{50} (µg/mL) of each previous oil, prepared by serial dilution. The survival of cancer was as follows: 0, 24, 48, 72 and 96 h. A 5 mg/mL MTT solution was added to each well, followed by a 4-hour incubation. Formazan crystals were solubilized using 100 µL of 99.9% DMSO, and absorbance was measured at 540 nm [23].

Scratch wound healing migration assay

Cell migration was assessed using a scratch wound healing assay, as described in [24]. B16F10 cells (2×10^5 cells/mL) were cultured in DMEM/F12 medium supplemented with 10% FBS and 1% penicillin streptomycin for 24 h in 60 mm culture plates at 37 °C with 5% CO_2 until reaching 80% - 90% confluence. A linear wound was created using 0.2 mL sterile pipette tips, and plates were washed twice with PBS (phosphate-buffered saline). Fresh medium containing the extract (50 and 100 µg/mL) was then added, while DMEM with 1% DMSO served as the negative control. After 4 h of incubation, images were captured using a phase-contrast microscope.

Wound confluence (%) = $(S_{0\ h} - S_{4\ h})/S_{0\ h}\times100\%$ where $S_{0\ h}$ and $S_{4\ h}$ were the width of the initial scratch wound at 0 h and the width of the scratch wound at 4 h, respectively.

Cell adhesion assay

A cell adhesion assay was used to measure cell adherence. B16-F10 melanoma cells were seeded into 96-well plates at a density of 10^4 cells/well in culture medium (DMEM-F12 supplemented with 10% FBS and 0.5% antibiotics) containing essential oils at concentrations of 0, 100 and 200 µg/mL. The cells were incubated at 37 °C with 5 % CO_2 for an hour. Following incubation, non-adherent cells were removed by discarding the medium, and the wells were washed three times with PBS. After that, 100 µL of DMEM-F12 medium containing 0.5 mg/mL MTT was added to each well to assess the number of adherent cells that were not washed away. After 3 h of incubation, the medium was taken out, and each well received 100 µL of DMSO to dissolve the formazan crystals. The plates were gently shaken, and absorbance was measured at 540 nm using an ELISA reader (ELISA Model HumaReader HS) [25].

$$\text{Adhesion (\%)} = OD_{sample}/OD_{control} \times 100. \quad (1)$$

Gas chromatography-mass spectrometry (GC-MS) analysis

The samples of both species were analyzed using a GC-MS system (GCMS QP2010 SE Shimadzu) according to the procedure outlined in the Assaggaf H *et al*. [26] study [27]. The device had a DB-5MS UI column, which was 30 m in length, 0.25 m in internal diameter, and 0.25 m in film thickness. Helium was used as the carrier gas at a constant flow rate of 1.0 mL/min. The injector temperature was maintained at 250 °C, while the oven temperature was programmed as follows: Initial hold at 50°C for 2 min, followed by a ramp of 5 °C/min to 100 °C, then 10 °C/min to 150 °C, and finally 25 °C/min to 250 °C. The total chromatographic run time was 22 min. Compound identification was achieved by comparing mass spectra with the NIST 2020 library and confirming retention indices (RI) calculated against a homologous series of n-alkanes (C8

- C20). The relative percentage of each component was determined by peak area normalization. Only % area values were reported in the results.

Molecular docking

The three-dimensional structures of BRAF kinase (PDB ID: 6XFP-B-Raf Proto-Oncogene, Serine/Threonine Kinase), NRAS (PDB ID: 8VM2-NRAS Q61K bound to GTP), AKT3 (PDB ID: 2X18-PH domain of human AKT3 protein kinase), FAK (PDB ID: 1MP8-Focal Adhesion Kinase) [28], and HDAC (PDB ID: 6WHO-Histone deacetylases complex with peptide macrocycles) were retrieved from the Research Collaboratory for Structural Bioinformatics Protein Data Bank (RCSB PDB). In the meantime, the molecular structures of 46 compounds were obtained from PubChem.

Virtual screening of these compounds against the target protein was performed using CB-Dock2 [29], a validated structure-based docking platform that incorporates cavity detection and AutoDock Vina docking. Prior to docking, CB-Dock2 automatically processed protein structures by removing non-amino acid residues and water molecules, adding polar hydrogens and missing atoms, and assigning atomic charges. Docking scores (binding free energy, kcal/mol) were used to rank the compounds according to their predicted binding affinity. The lowest binding energy pose (best binding affinity) for each protein-ligand complex was selected for further analysis. Molecular interactions were then visualized using Studio Discovery 2025 (2D interaction mapping).

Absorption, distribution, metabolism, excretion, and toxicity (ADMET) prediction

After molecular docking analysis, the top-ranked compounds were evaluated for their ADMET profiles. The chemical structures, including molecular formulas and canonical SMILES, were retrieved from PubChem (https://pubchem.ncbi.nlm.nih.gov/, accessed May 2025). The physicochemical and pharmacokinetic properties of the compounds were analyzed using SwissADME (http://www.swissadme.ch/, accessed May 2025) [30]. Drug-likeness was assessed according to Lipinski's Rule of Five criteria, which considers compounds with a molecular weight <500 g/mol, a log *p* value <5, <10 hydrogen bond acceptors, and <5 hydrogen bond donors as likely to be orally bioavailable [31]. Additionally, pharmacokinetic characteristics of compounds were collected by pkCSM (https://biosig.lab.uq.edu.au/pkcsm/prediction, accessed May 2025), which predicts key ADMET parameters including absorption, distribution, metabolism, excretion, and toxicity [26].

Identification of prediction targets for potential compounds

The potential target genes of the screened active compounds were identified using SwissTargetPrediction (http://www.swisstargetprediction.ch/, accessed May 2025), with the organism restricted to *Homo sapiens*. The predictive model of SwissTargetPrediction has been validated on an external test set of experimentally confirmed active compounds, demonstrating reliable performance. This platform infers potential targets based on molecular similarity to known bioactive compounds, integrating both 2D and 3D molecular descriptors. For subsequent analysis, only target genes with a predicted probability (P) greater than 0 were retained to ensure biological relevance [32].

Gene Ontology (GO) and Kyoto Encyclopedia of Genes and Genomes (KEGG)

Based on the predicted compound-gene associations and docking targets, Gene Ontology (GO) enrichment analysis was performed to investigate the functional roles of the identified genes within the regulatory network, and KEGG pathway enrichment analysis was conducted to determine the biological pathways associated with these target genes [33]. Both GO and KEGG analyses were performed using ShinyGO (https://bioinformatics.sdstate.edu/go/). *p* -values were calculated using the hypergeometric test, and false discovery rates (FDRs) were adjusted with the Benjamini-Hochberg method to correct for multiple testing. Fold enrichment was defined as the ratio between the proportion of genes in the query list mapped to a given pathway and the proportion of background genes in the same pathway. While FDR indicates the statistical significance of enrichment, fold enrichment reflects the effect size. An FDR threshold of $p \leq 0.05$ was applied to identify significantly enriched terms. The

top 10 enriched GO terms and KEGG pathways were selected for visualization as bubble plots [34].

Kaplan-meier survival analysis for signature genes

Kaplan-meier survival analysis of the signature genes was conducted using the GEPIA web tool (http://gepia.cancer-pku.cn/), which integrates data from TCGA and GTEx datasets [17]. Survival analysis for each gene in skin cutaneous melanoma (SKCM) was conducted using the log-rank (Mantel-Cox) test. Genes with $p \leq 0.05$ in univariate Cox regression were considered statistically significant. Patients were stratified into high-risk and low-risk groups based on the median risk score. Kaplan-Meier survival curves were generated to compare overall survival between the two groups. The analysis included calculation of the hazard ratio (HR), along with the corresponding 95% confidence intervals (CIs) and log-rank p values, to quantify the prognostic relevance of the signature genes [35].

Statistical analysis

All experiments were carried out a minimum of three times. The data were expressed as mean values with their corresponding standard deviations (SD). Statistical analysis and data processing were completed using Microsoft Excel 2016 and GraphPad Prism 9. All results were analyzed by unpaired Student's t-tests. The statistically significant differences were determined at $p \leq 0.05$ (*), $p \leq 0.01$ (**), $p \leq 0.001$ (***), and $p \leq 0.0001$ (****).

Results and discussion

Cytotoxicity activity

The cytotoxic activities of essential oils from various *Eucalyptus* species were evaluated against B16F10 murine melanoma cells using the MTT assay (**Figure 1**). The IC_{50} values were reported as follows: The standard anticancer drug doxorubicin exhibited an IC_{50} of 0.2179 µg/mL; *Eucalyptus camaldulensis* essential oil showed an IC_{50} of 182 µg/mL; and *Eucalyptus tereticornis* essential oil had an IC_{50} of 152.9 µg/mL. Although both essential oils were considerably less potent than doxorubicin, their cytotoxic effects are indicative of anticancer potential, consistent with the criteria proposed by Kuete *et al.* [36]. Notably, the IC_{50} values of the present extracts were lower than that reported for *Etlingera elatior* essential oil (IC_{50} = 214.85 ± 4.65 µg/mL), which contains major compounds such as caryophyllene (12.58%), humulene (15.21%), and caryophyllene oxide (2.82%). That study also reported inhibition of melanin content at 253.56 ± 3.65 µg/mL in B16F10 cells, corresponding to approximately threefold lower efficacy than standard anti-melanogenic compounds [37]. Furthermore, the cytotoxic activity observed in this study was greater than that reported for *Tetradenia riparia* (Hochst.) Codd essential oil, which exhibited an IC_{50} of 272.37 ± 18.45 µg/mL against B16F10 cells [38]. These results confirm that both essential oils exert cytotoxic activity against melanoma cells, especially *E. tereticornis*.

Importantly, despite the relatively high IC_{50} values, the major constituent of *Eucalyptus* essential oils, 1,8-cineole, has been widely recognized for its anti-inflammatory and antioxidant properties [8,10]. These biological activities are critical in the suppression of tumor progression, as they help modulate the tumor microenvironment and reduce chronic oxidative damage-a known contributor to cancer development [39]. Our data aligned with evidence from previous studies, reinforcing the anticancer potential of *Eucalyptus*-derived essential oils. For instance, *Eucalyptus globulus* essential oil exhibited potent cytotoxicity against B16F10 cells, with an IC_{50} of 5.23 µg/mL [40], highlighting its strong bioactivity in this cell line. Additionally, *E. camaldulensis* essential oil has shown cytotoxic effects on other cancer cell types, such as colorectal cancer Caco-2 cells, with an IC_{50} around 100 µg/mL [41]. This effect has been linked to apoptosis induction, potentially through modulation of apoptotic genes such as BAX and BCL-2 [41]. Moreover, *E. camaldulensis* flower essential oil has been reported to inhibit melanogenesis, potentially via its antioxidant activity and by downregulating mitogen-activated protein kinase (MAPK) and protein kinase A (PKA) signaling pathways [7]. Taken together, these findings suggest that *E. camaldulensis* and *E. tereticornis* may exert anticancer effects through multiple mechanisms, including direct cytotoxicity, apoptosis induction, antioxidant activity, and suppression of tumor-related signaling pathways such as MAPK. These multi-targeted actions highlight their potential as promising

candidates for further development in cancer therapeutics, particularly in the context of skin cancer.

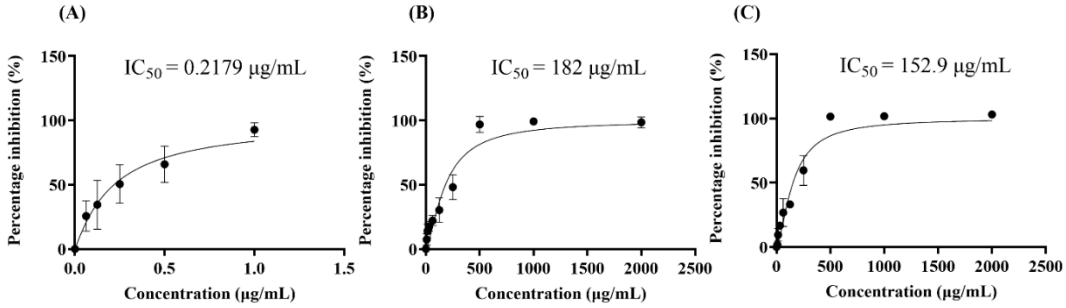

Figure 1 Cytotoxic activities of essential oils: (A) positive control (doxorubicin), (B) *E. camaldulensis*, and (C) *E. tereticornis.*

Timepoint effect of IC_{50} of essential oils

We further evaluated the time-dependent anticancer potential of *Eucalyptus* species by assessing their cytotoxic effects on B16F10 melanoma cells at 0, 24, 48, 72 and 96 h. As shown in **Figures 2(A) - 3(A)**, the untreated control cells exhibited a gradual increase in cell proliferation over time, from 0 to 96 h in the *E. camaldulensis* group and from 0 to 72 h in the *E. tereticornis* group. In contrast, treatment with either essential oil significantly reduced cell proliferation, particularly after 48 h, when cells were seeded at the same initial density (3×10^3 cells/well) at 0 h. This inhibitory effect was more clearly illustrated in **Figures 2(B) - 3(B)**, which show the percentage inhibition of cell growth over time. For *Eucalyptus camaldulensis*, the highest inhibition rate was observed at 48 and 72 h (~52%), followed by a slight decrease at 96 h (42.44%) (**Figure 2(B)**). In the case of *Eucalyptus tereticornis*, it showed its highest inhibition rate at 48 h (66.84%), which declined at 72 h (36.77%) and further decreased at 96 h (31.02%) (**Figure 3(B)**). Although *E. tereticornis* exhibited a delayed onset of cytotoxicity compared to *E. camaldulensis*, it demonstrated a stronger inhibitory effect at 72 h (36.77%) than *E. camaldulensis* at the same time point (~52%). This greater cytotoxic potential is consistent with the lower IC_{50} value of *E. tereticornis* (152.9 µg/mL), suggesting that it possesses higher intrinsic cytotoxic activity.

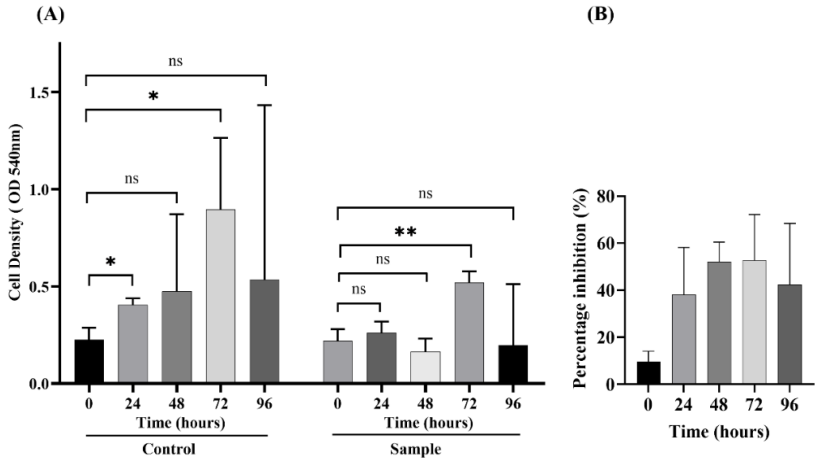

Figure 2 Timepoint effect on the B16F10 cell line of *E. camaldulensis*. (A) OD 540 nm of B16F10 cell line, (B) Percentage inhibition of B16F10 cell line. The result was analyzed by unpaired Student's t-tests. The statistically significant differences were determined at $p \leq 0.05$ (*), $p \leq 0.01$ (**), and ns means not significant (compared to the normal control group).

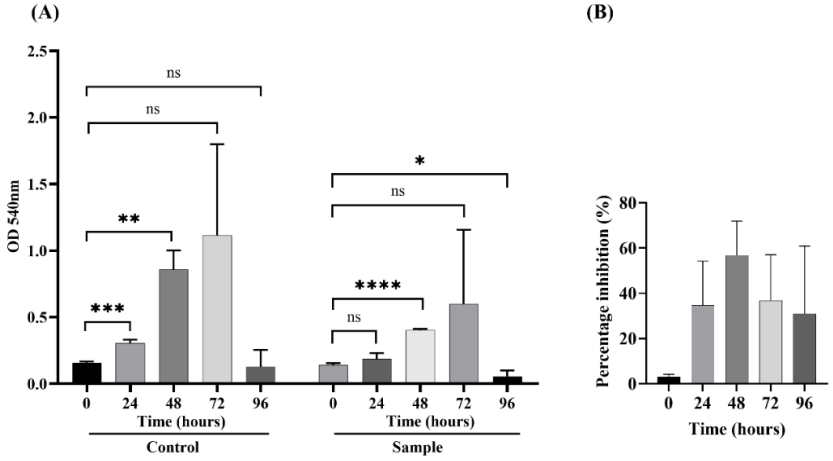

Figure 3 Timepoint effect on the B16F10 cell line of *E. tereticornis*. (A) OD 540 nm of B16F10 cell line, (B) Percentage inhibition of B16F10 cell line. The result was analyzed by unpaired Student's t-tests. The statistically significant differences were determined at $p \leq 0.05$ (*), $p \leq 0.01$ (**), $p \leq 0.001$ (***), and $p \leq 0.0001$ (****), and ns means not significant (compared to the normal control group).

Scratch wound healing migration assay

The migration of B16F10 melanoma cells was evaluated using a wound healing assay. Cells were treated with the test compound at a concentration that inhibited cancer cell viability by less than 1%. Representative images on the left illustrate wound closure over time, while the bar graph on the right quantitatively presents the percentage of cell migration. In the negative control, cells exhibited a high migration rate in both essential oils. For *Eucalyptus camaldulensis*, at 50 µg/mL, the migration rate was markedly reduced to about 11.375% compared to 36.871% in the negative control ($p < 0.05$), indicating statistically significant inhibition (**Figure 4(A)**). However, at 100 µg/mL, the migration rate slightly increased to 22.459%, though it remained lower than the control. In contrast, *E. tereticornis* exhibited stronger inhibition of migration. At 50 µg/mL, the migration rate was similar to *E. camaldulensis* at 12.605%, but at 100 µg/mL, it further decreased to 6.449%, showing a more potent inhibitory effect (**Figure 4(B)**). Thus, these results support the potential of *Eucalyptus camaldulensis* and *Eucalyptus tereticornis* essential oils as inhibitors of melanoma cell migration, with *E. tereticornis* showing stronger efficacy at higher doses.

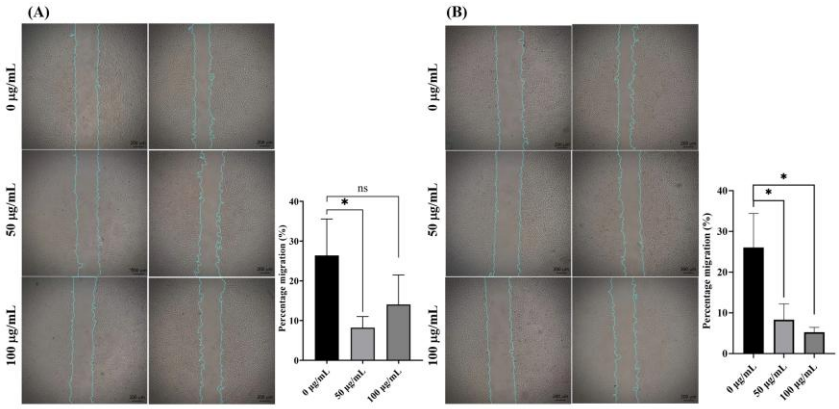

Figure 4 Migration inhibitory activity of essential oils on the B16F10 cell line: (A) *E. camaldulensis* and (B) *E. tereticornis.* The result was analyzed by unpaired Student's t-tests. The statistically significant differences were determined at $p \leq 0.05$ (*), ns means not significant (compared to the normal control group).

Cell adhesion assay

An adhesion assay was employed to evaluate B16F10 melanoma cell adhesion following treatment with the test compounds at concentrations that did not significantly affect cell viability (<1% inhibition). When the concentrations of *Eucalyptus camaldulensis* and *Eucalyptus tereticornis* essential oils increased from 0 µg/mL to 100 µg/mL, a significant reduction in B16F10 cell adhesion was observed ($p < 0.05$) (**Figure 5**). This suggests that both essential oils can interfere with the adhesion of B16F10 melanoma cells, thereby reducing their ability to attach to the surface. The concentration-dependent decrease in cell adhesion indicates that both essential oils may disrupt cell-substrate interactions-an essential step in preventing cancer metastasis.

E. camaldulensis and *E. tereticornis* demonstrate greater efficacy in reducing cancer cell adhesion and migration, which are critical steps in metastasis. According to the study by Huang *et al*. [7], *Eucalyptus* essential oils, including those from *E. camaldulensis*, exhibit antioxidant, anti-melanogenic, and cytotoxic effects on B16F10 melanoma cells, indicating their ability to modulate cellular behavior and signaling pathways involved in adhesion and metastasis [7]. In addition to confirming the known anticancer effects of *E. camaldulensis*, our study further demonstrates that *E. tereticornis*-a member of the *Eucalyptus* genus-also shows strong potential in combating skin cancer. This is evidenced by its low IC_{50} value, strong inhibition of cell migration, and significant reduction in cell adhesion.

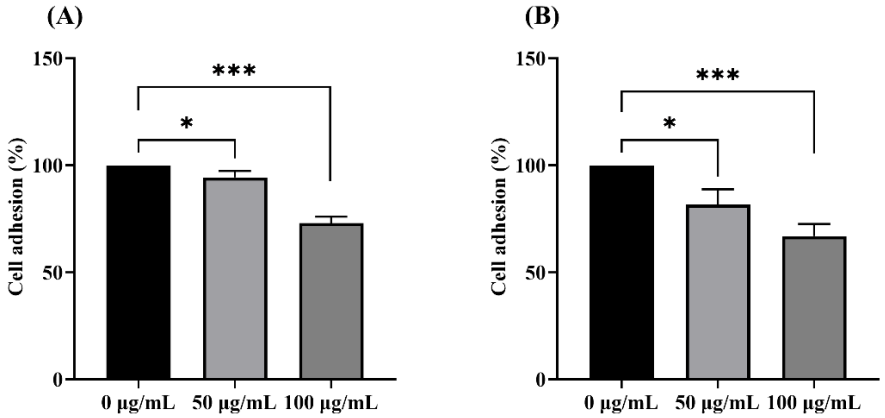

Figure 5 Cell adhesion of B16F10, (A) *E. camaldulensis*, and (B) *E. tereticornis.* The result was analyzed by unpaired Student's t-tests. The statistically significant differences were determined at $p \leq 0.05$ (*), $p \leq 0.001$ (***).

Gas chromatography-mass spectrometry (GC-MS) analysis

The GC-MS analysis of essential oils from two *Eucalyptus* species identified a total of 46 volatile compounds (0.24% to 16.34%) (**Table 1**, **Figure 1 - 2(S)**). These major compounds are highlighted in bold in **Table 1**. For *E. camaldulensis*, the main constituents were β-eudesmol (16.34%), γ-terpinene (12.59%), o-cymene (11.49%), eucalyptol (9.90%), and α-phellandrene (8.66%). For the *E. tereticornis* sample, the primary components included β-pinene (15.88%), caryophyllene oxide (14.39%), α-pinene (13.73%), eucalyptol (10.13%), and spathulenol (7.32%). Among these, ten compounds were also found in the essential oils from both *E. camaldulensis* and *E. tereticornis*, such as α-pinene, β-pinene, eucalyptol, and d-limonene-compounds frequently found in *Eucalyptus* essential oils and known for their therapeutic properties [7,42]. Previous studies have suggested that these constituents may contribute to anticancer activities, including melanoma inhibition, metastasis prevention, sensitization to antitumor agents, chemoprevention, and regulation of melanogenesis [43].

Notably, the two species exhibited distinct sesquiterpene profiles. *E. camaldulensis* contained substantial amounts of β-eudesmol (16.34%), γ-terpinene (12.59%), *o*-cymene (11.49%), α-phellandrene (8.66%), and γ-eudesmol (7.97%), whereas *E. tereticornis* was characterized by higher levels of caryophyllene oxide (14.39%), *p*-cymene (4.20%), and spathulenol (7.32%). In a previous study by Yang *et al.* [44], β-caryophyllene-an isomer of

caryophyllene abundantly present in *E. tereticornis*-was demonstrated to reduce melanin production in B16F10 melanoma cells and suppress melanogenesis by downregulating the expression of MITF, TRP-1, TRP-2, and tyrosinase [44]. Furthermore, essential oils from *Alpinia nantonensis*, which contain major constituents such as α-pinene (4.23% - 8.28%) and *d*-limonene (2.43% - 2.50%), showed similarities to *E. tereticornis* in terms of α-pinene (13.73%) and *d*-limonene (6.54%) content. These compounds exhibited strong inhibitory effects on melanin synthesis and cellular tyrosinase activity in forskolin-stimulated cells by downregulating TYR and TRP-1 expression, suppressing MITF, and modulating the PI3K/AKT signaling pathway [45]. Overall, the observed differences in chemical composition between the two *Eucalyptus* species may be influenced by geographic and environmental factors, which in turn affect their anticancer and antimelanogenic potential [46]. Consequently, although both species contain promising bioactive compounds, their therapeutic efficacy and potential applications may vary due to intrinsic chemical diversity and environmental influences.

Table 1 Comparison of the chemical components of the essential oil from *E. camaldulensis* and *E. tereticornis.*

No	Major components	CID	*E. camaldulensis*		*E. tereticornis*	
			Retention time	Area (%)	Retention time	Area (%)
1	α-Thujene	17868	4.517	0.28	9.422	2.98
2	1,3,3-Trimethylbicyclo[2.2.1]hept-2-yl acetate	107217	-	-	9.787	0.49
3	2,3-Pinanediol	62044	11.701	0.90	-	-
4	2-Carene	79044	6.031	1.02	-	-
5	4-Carene	530422	7.277	1.72	-	-
6	5-Isopropyl-6-methyl-hepta-3,5-dien 2-ol	5363138	10.294	0.33	-	-
7	6,6-Dimethyl-2 methylenebicyclo[3.1.1]heptan-3-one	9585226	-	-	8.800	0.87
8	Agarospirol	21675005	17.169	1.85	-	-
9	Alloaromadendrene	10899740	13.886	0.94	13.890	4.16
10	α-Caryophyllene	5281520	14.181	0.59	-	-
11	α-Copaene	19725	12.746	0.51	-	-
12	α-Guaiene	5317844	-	-	14.263	1.50
13	**α-Phellandrene**	**7460**	**5.863**	**8.66**	-	-
14	**α-Pinene**	**6654**	4.671	4.93	**4.667**	**13.73**
15	α-Selinene	10856614	14.850	0.35	-	-
16	α-Terpineol	17100	9.376	2.11	9.375	1.20
17	α-Terpineol acetate	111037	-	-	12.127	0.94
18	Aristolene	530421	17.095	1.06	-	-
19	β-Caryophyllene	5281515	13.568	1.91	13.570	2.20
20	**β-Eudesmol**	**91457**	**17.475**	**16.34**	-	-
21	β-Linalool	6549	7.468	0.26	-	-
22	β-Myrcene	31253	5.468	1.06	5.470	0.24

No	Major components	CID	*E. camaldulensis*		*E. tereticornis*	
			Retention time	Area (%)	Retention time	Area (%)
23	**β-Pinene**	**440967**	5.408	4.93	**5.408**	**15.88**
24	β-Selinene	442393	14.750	0.59	-	-
25	Bicylo[4.1.0]heptane,7 bicyclo[4.1.0]hept-7-ylidene	562714	-	-	14.194	1.39
26	Borneol	6552009	-	-	8.988	0.89
27	Bornyl acetate	6448	-	-	11.037	0.30
28	Camphene	6616	-	-	4.950	1.97
29	**Caryophyllene oxide**	**1742210**	**-**	**-**	**16.314**	**14.39**
30	Caryophyllene-(l1)	5369754	-	-	16.495	1.85
31	D-Fenchyl alcohol	15406	-	-	7.960	1.31
32	D-Limonene	440917	6.267	3.95	6.251	6.54
33	Epiglobulol	11858788	-	-	15.955	0.86
34	**Eucalyptol**	**2758**	**6.356**	**9.90**	**6.336**	**10.13**
35	γ-Eudesmol	6432005	17.043	7.97	-	-
36	**γ-Terpinene**	**7461**	**6.791**	**12.59**	-	-
37	Ledol	92812	-	-	16.659	1.30
38	L-trans-Pinocarveol	1201530	-	-	8.402	1.95
39	**o-Cymene**	**10703**	**6.192**	**11.49**	-	-
40	Palustrol (Ledum)	110745	-	-	16.100	0.44
41	p-Cymene	7463	-	-	6.162	4.20
42	Phytol	5280435	23.372	0.40	-	-
43	Sabinyl acetate	94266	9.546	0.54	-	-
44	**Spathulenol**	**92231**	**-**	**-**	**16.190**	**7.32**
45	Spiro(4,5)decane	135982	-	-	16.740	0.60
46	Terpinen-4-ol	11230	9.123	2.83	9.119	0.36

Molecular docking

Due to the intriguing yet not fully understood selective cytotoxicity of essential oils on cancer, we conducted an *in silico* study using molecular docking approaches to evaluate all chemical constituents from two essential oils against a panel of cancer-related target proteins. The selected targets are involved in key oncogenic signaling pathways, including the MAPK/ERK pathway, RAS-RAF-MEK-ERK signaling, the PI3K/AKT/mTOR pathway, FAK/integrin signaling, and epigenetic regulation via HDACs [28].

The docking results, summarized in **Table 2**, reveal several compounds with promising binding affinities. The top seven compounds with the most favorable docking scores were further visualized using Discovery Studio 2025 (**Figure 6**). Interestingly, these seven compounds all showed significant binding to BRAF, a critical kinase in the MAPK/ERK signaling cascade, which plays a pivotal role in melanoma progression [47]. All seven compounds exhibited binding energies ≤ −8.1 kcal/mol, indicating stable and potentially effective interactions [48].

Among the top hits, bicyclo[4.1.0]heptane, 7-bicyclo[4.1.0]hept-7-ylidene (1.39% in *Eucalyptus*

tereticornis essential oil), displayed the strongest binding affinity toward BRAF, with a docking score of −8.5 kcal/mol. Molecular interactions included Pi-Alkyl interactions with TRP_A:531 and PHE_A:595; Pi-Sigma: PHE_A:583; Alkyl interactions with CYS_A:532; ALA_A:481; LYS_A:483 and VAL_A:471; and Van der Waals interactions with LEU_A:514; ASP_A:594; ILE_A:463; GLN_A:530 and THR_A:529.

Another compound from *E. tereticornis*, caryophyllene-(l1) (1.85%), ranked second and showed strong interaction with BRAF. In contrast, compounds from *Eucalyptus camaldulensis*, such as α-copaene (0.51%) and α-caryophyllene (0.59%), demonstrated moderate binding affinities to BRAF. Interestingly, alloaromadendrene, present in both species but at a higher concentration in *E. tereticornis* (4.16%), interacted with both FAK and BRAF, indicating dual-targeting potential.

Although the anticancer potential of *Eucalyptus* essential oils has been reported previously, to the best of our knowledge, this is the first study to comprehensively explore the molecular docking-based interaction profiles of volatile constituents from *E. camaldulensis* and *E. tereticornis* against melanoma-associated protein targets. The docking analysis strongly supports the experimental cytotoxicity findings by demonstrating that multiple essential oil components interact effectively with proteins critically involved in melanoma pathogenesis, particularly BRAF. Interestingly, alloaromadendrene, present in both species but at a higher concentration in *E. tereticornis* (4.16%), interacted with both FAK and BRAF, indicating dual-targeting potential. Consistent with these findings, previous studies have reported that β-caryophyllene-a sesquiterpene isomer structurally related to caryophyllene-(l1)-exhibits significant interactions with PI3K and AKT proteins and downregulates the PI3K/AKT signaling pathway, which regulates key cellular processes such as proliferation, survival, and angiogenesis. Moreover, β-caryophyllene has been shown to induce apoptosis through suppression of PI3K/AKT signaling and ROS-mediated activation of MAPK pathways, further supporting the biological relevance of caryophyllene-related compounds in cancer therapy [49,50].

Overall, the molecular docking results indicate that *E. tereticornis* essential oil contains a greater number of bioactive constituents with strong and/or multitarget interactions with key melanoma-related proteins. These findings provide a mechanistic basis for further investigation of *E. tereticornis* as a promising candidate for targeting the MAPK/ERK signaling pathway in the development of anti-melanoma therapeutics [47]. Nevertheless, further experimental validation is required to confirm the functional relevance of these *in silico* predictions. Specifically, assessment of pathway-related biomarkers-such as phosphorylated ERK (pERK), phosphorylated AKT (pAKT), and FAK phosphorylation levels-using Western blot or related techniques would be essential to verify whether these signaling pathways are effectively modulated in melanoma cells.

Table 2 Docking results of top-ranked potential drug compounds with target proteins by CB-Dock2.

Protein	Ligand	Docking score	Interaction	Amino acids (position of interaction)
BRAF	Bicylo[4.1.0]heptane,7 bicyclo[4.1.0]hept-7-ylidene	–8.5	Pi-Alkyl	TRP_A:531, PHE_A:595
			Pi-Sigma	PHE_A:583
			Alkyl	CYS_A:532, ALA_A:481, LYS_A:483, VAL_A:471
			Van der Waals	LEU_A:514, ASP_A:594, ILE_A:463, GLN_A:530, THR_A:529
FAK	Alloaromadendrene	–8.2	Pi-Alky	HIS_A:574
			Alkyl	LEU_A:505, LEU_A:597, VAL_A:504
			Van der Waals	ASP_A:594, GLY_A:593, ILE_A:592, ILE_A:513, THR_A:508, LEU_A:567, ILE_A:572, ILE_A:573
BRAF	α-Copaene	–8.2	Pi-Alkyl	PHE_A:595

Protein	Ligand	Docking score	Interaction	Amino acids (position of interaction)
			Alkyl	LEU_A:514, LYS_A:483, ALA_A:482, PHE_A:595, VAL_A:471
			Van der Waals	VAL_A:482, ILE_A:527, THR_A:529, GLN_A:530, CYS_A:532, TRP_A:531
BRAF	Palustrol (Ledum)	–8.2	Pi-Alkyl	PHE_A:595
			Alkyl	VAL_A:471, ILE_A:463, ALA_A:481
			Van der Waals	LYS_A:483, LEU_A:514, THR_A:529, GLN_A:530, CYS_A:532, PHE_A:583, TRP_A:531
BRAF	Caryophyllene-(l1)	–8.2	Pi-Alkyl	PHE_A:595
			Pi-Sigma	TRP_A:531
			Alkyl	VAL_A:471, ALA_A:481, CYS_A:532
			Van der Waals	LEU_A:514, THR_A:529, LYS_A:483, ASP_A:594, GLY_A:464, ILE_A:463, PHE_A:583
BRAF	α-Caryophyllene	–8.1	Pi-Alkyl	PHE_A:595
			Pi-Sigma	TRP_A:531
			Alkyl	LYS_A:483, VAL_A:471, ALA_A:481, CYS_A:532
			Van der Waals	LEU_A:514, THR_A:529, GLY_A:464, ILE_A:463, THR_A:599
			Pi-Alkyl	PHE_A:595
BRAF	Alloaromadendrene	–8.1	Pi-Alkyl	HIS_A:574
			Van der Waals	GLU_A:501, ASP_A:594, GLY_A:593, ILE_A:592, ILE_A:513, THR_A:508, LEU_A:567, ILE_A:572, ILE_A:573
			Alkyl	LEU_A:505, LEU_A:597, VAL_A:504

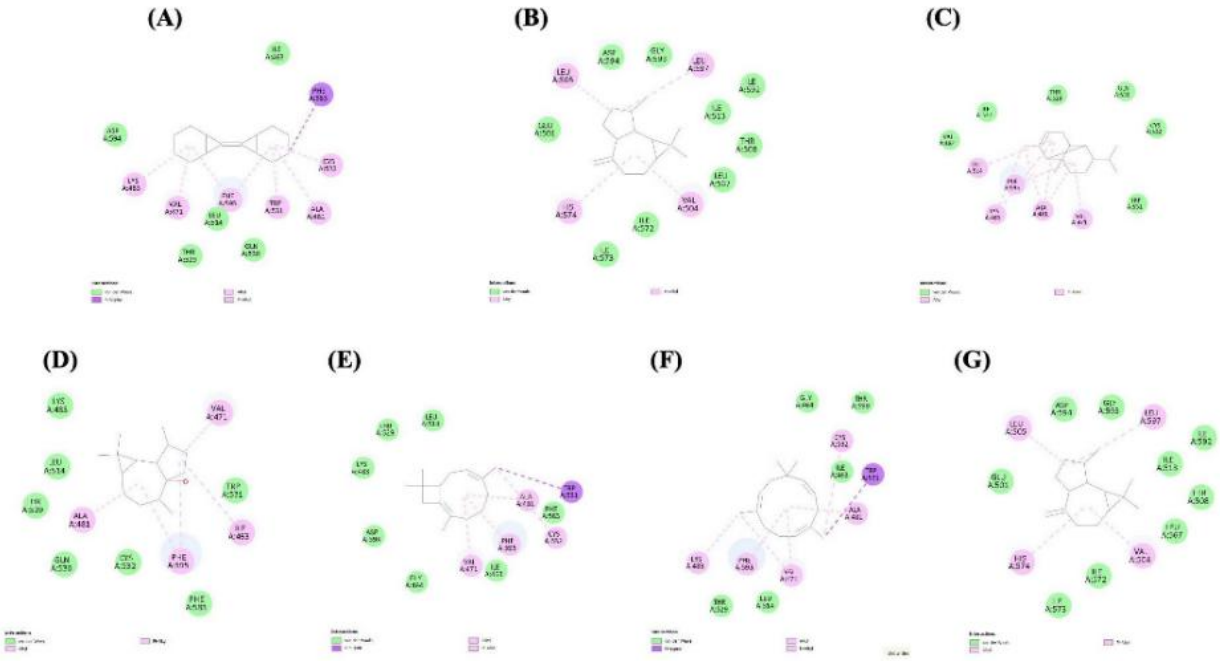

Figure 6 Interaction: BRAF and bicylo[4.1.0]heptane,7 bicyclo[4.1.0]hept-7-ylidene (A), FAK and alloaromadendrene (B), BRAF and α-copaene (C), BRAF and palustrol (Ledum) (D), BRAF and caryophyllene-(l1) (E), BRAF and α-caryophyllene (F), BRAF and alloaromadendren and (G) 2D model.

Absorption, distribution, metabolism, excretion, and toxicity (ADMET) analysis

In this study, the top six compounds with the highest docking scores were further evaluated for their drug-like properties, including biological activity, safety, efficacy, and pharmacokinetic characteristics, particularly focusing on absorption, distribution, metabolism, excretion, and toxicity (ADMET) [30]. According to the swissADME analysis, all compounds violated Lipinski's based on the MLOG > 4.15 criterion, except for palustrol. As noted by Manhanthesh MT *et al*. (2020), compounds that fail more than two Lipinski criteria are generally considered less likely to exhibit good intestinal absorption [51,52]. In our analysis, although most compounds showed a violation in MLOGP, they still satisfied the remaining Lipinski parameters, indicating that they can be considered as partially compliant with Lipinski's Rule of Five (**Table 3**) [31].

In addition, ADMET predictions using pkCSM were summarized in **Table 4**, all compounds demonstrated high predicted human intestinal absorption (HIA > 93%), suggesting strong potential for digestive absorption. Most compounds also showed blood-brain barrier (BBB) permeability, with Log BB values >0.3, indicating the capacity to penetrate the central nervous system (CNS). Additionally, all compounds exhibited CNS permeability within the acceptable range (–1 to –3 Log PS), implying potential applicability in CNS-related therapeutic targets. In terms of metabolism, compound C4 showed no predicted interaction with cytochrome P450 (CYP) enzymes. Compound C1 was predicted to be both a substrate and an inhibitor of CYP2D6, CYP3A4, or CYP1A2. Similarly, C5 was predicted to act as both a substrate and inhibitor of CYP3A4 and CYP1A2. In contrast, C2 and C6 were identified as substrates of CYP2D6 and CYP3A4, respectively. C3 was predicted to be a substrate for both CYP2D6 and CYP3A4. Regarding toxicity, none of the compounds were predicted to be hepatotoxic. However, skin sensitization was observed in C4 - C6, suggesting a potential risk of allergic reactions, which should be addressed during future drug development.

Overall, despite minor safety concerns in a subset of compounds, the ADMET profiles indicate favorable pharmacokinetic and drug-like characteristics for most candidates, supporting their potential for further development as therapeutic agents.

Table 2 The prediction of physicochemical properties of six compounds, based on Lipinski rules by SwissADME.

			Physico-Chemical properties							**Lipinski rules**
Compound Numbers	**Name compound**	**CID**	**Formula**	**Molecular weight (g/mol)**	**Molar refractive index**	**Rotatable bonds**	**Log P (Octanol/Water)**	**HBA**	**HBD**	**Categorical (Yes/No)**
	Rule			≤ 500	40 ≤ MR ≤ 130	≤ 10	<5	≤ 10	<5	Yes/No
C1	Bicylo[4.1.0]heptane,7 bicyclo[4.1.0]hept-7-ylidene	562714	C14H20	188.31	60.48	0	5.39	0	0	Yes, 1 violation, MLOGP>4.15
C2	Alloaromadendrene	10899740	C15H24	204.35	67.14	0	5.65	0	0	Yes, 1 violation, MLOGP>4.15
C3	α-Copaene	19725	C15H24	204.35	67.14	1	5.65	0	0	Yes, 1 violation, MLOGP>4.15
C4	Palustrol (Ledum)	110745	C15H26O	222.37	68.82	0	3.81	1	1	Yes, 0 violation

C5	Caryophyllene-(l1)	5369754	C15H24	204.35	68.78	0	4.63	0	0	Yes, 1 violation, MLOGP>4.15
C6	α-Caryophyllene	5281520	C15H24	204.35	70.42	0	4.53	0	0	Yes, 1 violation, MLOGP>4.15

Table 3 The prediction of ADMET *in silico* pharmacokinetic properties of six compounds by pkCSM.

Compound					1	2	3	4	5	6
Absorption	**HIA**			**Numeric (% Absorbed)**	95.771	95.302	96.221	93.979	94.755	94.682
	Caco 2			**Numeric (log Papp in 10^{-6} cm/s)**	1.384	1.395	1.374	1.496	1.416	1.421
	Skin Permeability			**Numeric (Log Kp)**	–2.379	–1.828	–2.225	–2.247	–1.571	–1.739
Distribution	**BBB**			**Numeric (Log BB)**	0.891	0.822	0.887	0.617	0.726	0.663
	CNS			**Numeric (Log PS)**	–1.106	–1.769	–1.659	–2.536	–2.172	–2.555
Metabolism	**Substrate**		**2D6**	**Categorical (Yes/No)**	Yes	Yes	Yes	No	No	No
			3A4		Yes	No	Yes	No	Yes	Yes
	Inhibitor	**Cytochromes**	**1A2**		Yes	No	No	No	Yes	No
			2C19		No	No	No	Yes	No	No
			2C9		No	No	No	Yes	No	No
			2D6		No	No	No	No	No	No
			3A4		No	No	No	No	No	No
Excretion	**TRC**			**Numeric (Log mL/min/kg)**	1.032	0.926	0.95	0.856	1.065	1.282
Toxicity	**AMES Toxicity**			**Categorical (Yes/No)**	No	No	No	No	No	No
	Hepatotoxicity				No	No	No	No	No	No
	Skin Sensitization				No	No	No	Yes	Yes	Yes

Abbreviations: HIA = Intestinal Absorption Human; Caco 2 = Caco 2 Permeability; BBB = blood-brain barrier Permeability; CNS = central nervous system; TRC = Total renal clearance.

Networking pharmacology

To further elucidate the molecular mechanisms underlying the anticancer potential of compounds from *Eucalyptus camaldulensis* and *Eucalyptus tereticornis*, target prediction was performed using the SwissTargetPrediction database (limited to *Homo sapiens*), yielding potential human target genes (**Table 3(S)**). These targets were subsequently subjected to Gene Ontology (GO) and KEGG pathway enrichment analyses to explore their functional significance (**Figure 3(S)**).

For bicyclo[4.1.0]heptane, 7-bicyclo[4.1.0]hept-7-ylidene, GO analysis identified 58 statistically significant terms ($p < 0.05$), comprising 27 biological process (BP) terms, 6 cellular component (CC) terms, and 25 molecular function (MF) terms. For alloaromadendrene, a total of 311 significant GO terms were identified, including 273 BP, 11 CC, and 27 MF terms. α-copaene was associated with 501 enriched GO

terms, distributed across 363 BP, 35 CC, and 103 MF categories. Palustrol (ledum) yielded 146 significant GO terms, including 112 BP, 6 CC, and 28 MF terms. Notably, caryophyllene-(l1) demonstrated the most extensive enrichment, with 1,136 significant GO terms, including 1,000 BP, 14 CC, and 122 MF terms.

The most significantly enriched biological processes and molecular functions among all compounds included pathways related to lipid metabolism, steroid metabolism, glucuronosyltransferase activity, UDP-glycosyltransferase activity, and lipid oxidation. According to Dellinger *et al*. [53], UDP-glucuronosyltransferases (UGTs) play a critical role in anticancer drug detoxification and metabolism. In particular, inhibition of UGT2B7 has been shown to enhance the sensitivity of WM115 melanoma cells to afriamycin and epirubicin. This observation aligns with our predicted target genes, especially for bicyclo[4.1.0]heptane, 7-bicyclo[4.1.0]hept-7-ylidene; alloaromadendrene; and palustrol, all of which were associated with UGT-related pathways [53]. In addition, metabolic reprogramming of lipid processes plays an essential role in melanoma progression and therapy resistance. This includes lipid metabolism, lipid oxidation, and enzymes such as LPCAT1, which converts lysophosphatidylcholine to phosphatidylcholine and promotes oncogenic signaling through membrane lipid remodeling. Similarly, Yoshio Yamauchi *et al*. [54] demonstrated that SREBP regulates cholesterol and fatty acid biosynthesis and modulates PI3K-AKT-mTORC1 signaling in human melanoma cells; inhibition of this axis contributes to attenuation of tumor development [54].

Analysis shows strong localization to endoplasmic reticulum (ER), ER membrane, and presynaptic membrane. During melanin synthesis, tyrosinase folds in the ER before melanosome transport; ER stress disrupts this folding, cutting tyrosinase levels and inhibiting melanin production in melanocytes [55]. ER and presynaptic enrichments point to protein folding responses (e.g., UPR) and signaling cascades.

KEGG pathway enrichment further highlighted key pathways such as cancer pathway, chemical carcinogenesis-receptor activation, chemical carcinogenesis-DNA adducts, and broad cancer-associated signaling pathways, suggesting the relevance of these compounds in modulating gene networks implicated in carcinogenesis.

Kaplan-meier survival analysis for signature genes

After assessing the survival status of signature genes associated with skin cutaneous melanoma (SKCM) from TCGA datasets in relation to the six top-scoring compounds from molecular docking analysis, we observed that the high-risk subpopulation exhibited significantly poorer survival outcomes compared to the low-risk group (**Figure 4(S)**). Among these compounds, two derived from *Eucalyptus tereticornis* showed statistically significant associations with skin cancer prognosis ($p < 0.05$): Alloaromadendrene (log-rank $p = 0.015$) and caryophyllene-(l1) (log-rank $p = 0.0096$). Both compounds were present at relatively high levels in *E. tereticornis*, particularly alloaromadendrene, which accounted for 4.16% of the essential oil composition (ranking sixth in its compound profile), compared to only 0.94% in *E. camaldulensis*. These results indicate that the target genes influenced by alloaromadendrene and caryophyllene-(l1) have a significant impact on melanoma patient survival. This finding supports the therapeutic potential of *E. tereticornis*, suggesting it may exert targeted anticancer effects through specific bioactive compounds.

Together, these findings demonstrate that *E. tereticornis* essential oil harbors phytochemical constituents with both predicted molecular efficacy and clinical relevance in melanoma. The dual evidence from gene pathway enrichment and survival analysis highlights a strong rationale for further investigation of compounds such as alloaromadendrene and caryophyllene-(l1) as potential lead structures in the development of plant-derived therapeutics for skin cancer. Future studies should validate these predictions through *in vitro* and *in vivo* models to assess their efficacy, safety, and mechanism of action in a melanoma context.

Conclusions

This study reveals that essential oils from *E. camaldulensis* and *E. tereticornis* possess anticancer activities. *E. tereticornis* oil demonstrated superior cytotoxicity against B16F10 melanoma cells and inhibited cell migration and adhesion. GC-MS analysis

identified key compounds, including β-pinene and caryophyllene oxide, while molecular docking supported their potential anticancer effects. These findings suggest that *E. tereticornis* essential oil holds promise as a natural agent for melanoma treatment, meriting further investigation.

Declaration of Generative AI in Scientific Writing

The authors acknowledge the use of generative AI tools (for example, ChatGPT by OpenAI) in the preparation of this manuscript, specifically for language editing and grammar correction. No content generation or data interpretation was performed by AI. The authors take full responsibility for the content and conclusions of this work.

CRediT Author Statement

Viet Hoang: Conceptualization, Project administration, Writing – review & editing; **Thang Truong Le:** Conceptualization, Experiment design, Writing – original draft, Writing – review & editing; **Tran Hoang Ngau:** Project administration, Data curation, Formal analysis, Writing – original draft, Writing – review & editing; **Chau Dao Minh Huynh:** Data curation, Formal analysis, Writing – original draft, Writing – review & editing; **Hoai Nguyen Thi Thanh:** Data curation, Formal analysis; **Ngan Phan Thu:** Data curation, Formal analysis; **Tran Ngo Bao Huynh:** Data curation, Formal analysis. All authors have read and agreed to the published version of the manuscript.

References

[1] AH Roky, MM Islam, AMF Ahasan, MS Mostaq, MZ Mahmud, MN Amin and MA Mahmud. Overview of skin cancer types and prevalence rates across continents. *Cancer Pathogenesis and Therapy* 2025; **3(2)**, 89-100.

[2] W Mingyue, G Xinghua and Z Li. Recent global patterns in skin cancer incidence, mortality, and prevalence. *Chinese Medical Journal* 2025; **138(2)**, 185-192.

[3] RL Siegel, TB Kratzer, AN Giaquinto, H Sung and A Jemal. Cancer statistics, 2025. *CA: A Cancer Journal for Clinicians* 2025; **75(1)**, 10-45.

[4] N Chandorkar, S Tambe, P Amin and C Madankar. A systematic and comprehensive review on current understanding of the pharmacological actions, molecular mechanisms, and clinical implications of the genus *Eucalyptus*. *Phytomedicine Plus* 2021; **1(4)**, 100089.

[5] L Alonso, J Picos and J Armesto. Mapping *Eucalyptus* species using worldview 3 and random forest. *The International Archives of the Photogrammetry, Remote Sensing and Spatial Information Sciences* 2022; **2022**, 819-825.

[6] H Khazraei, SA Shamsdin and M Zamani. *In vitro* cytotoxicity and apoptotic assay of *Eucalyptus globulus* essential oil in colon and liver cancer cell lines. *Journal of Gastrointestinal Cancer* 2022; **53**, 363-369.

[7] HC Huang, YC Ho, JM Lim, TY Chang, CL Ho and TM Chang. Investigation of the anti-melanogenic and antioxidant characteristics of *Eucalyptus camaldulensis* flower essential oil and determination of its chemical composition. *International Journal of Molecular Sciences* 2015; **16(5)**, 10470-10490.

[8] Y Huang, M An, A Fang, OJ Olatunji and FN Eze. Antiproliferative activities of the lipophilic fraction of *Eucalyptus camaldulensis* against MCF-7 breast cancer cells, UPLC-ESI-QTOF-MS metabolite profile, and antioxidative functions. *ACS Omega* 2022; **7(31)**, 27369-27381.

[9] Anju, A Kumar and P Yadav. Chemical composition, *in vitro* and *in silico* evaluation of essential oil from *Eucalyptus tereticornis* leaves for lung cancer. *Natural Product Research* 2023; **37(10)**, 1656-1661.

[10] B Dey and A Mitra. Chemo-profiling of eucalyptus and study of its hypoglycemic potential. *World Journal of Diabetes* 2013; **4(5)**, 170-176.

[11] AK Dhakad, VV Pandey, S Beg, JM Rawat and A Singh. Biological, medicinal and toxicological significance of *Eucalyptus* leaf essential oil: A review. *Journal of the Science of Food and Agriculture* 2018; **98(3)**, 833-848.

[12] B Rodenak-Kladniew, A Castro, P Stärkel, M Galle and R Crespo. 1,8-Cineole promotes G0/G1 cell cycle arrest and oxidative stress-induced senescence in HepG2 cells and sensitizes cells to anti-senescence drugs. *Life Sciences* 2020; **243**, 117271.

[13] ND Kien, G Jansson, C Harwood and C Almqvist. Clonal variation and genotype by environment interactions in growth and wood density in *Eucalyptus camaldulensis* at three contrasting sites in Vietnam. *Silvae Genetica* 2010; **59(1)**, 17-28.

[14] HD Manh, DT Hue, NTT Hieu, DTT Tuyen and OT Tuyet. The mosquito larvicidal activity of essential oils from *Cymbopogon* and *Eucalyptus* species in Vietnam. *Insects* 2020; **11(2)**, 128.

[15] DNX Lâm, NT Nhựt, VTB Ngọc, TT Trĩnh and LHH Hạ. Chemical composition and current use trend of essential oils from leaves of genus eucalyptus (*Eucalyptus sp*.) in Vietnam and the world: A review. *Cantho Journal of Medicine and Pharmacy* 2022; **46**, 145-154.

[16] XY Meng, HX Zhang, M Mezei and M Cui. Molecular Docking: A powerful approach for structure-based drug discovery. *Current Computer-Aided Drug Design* 2011; **7(2)**, 146-157.

[17] Z Tang, C Li, B Kang, G Gao, C Li and Z Zhang. GEPIA: A web server for cancer and normal gene expression profiling and interactive analyses. *Nucleic Acids Research* 2017; **45(1)**, 98-102.

[18] The Gene Ontology Consortium. Gene Ontology Consortium: Going forward. *Nucleic Acids Research* 2015; **43(1)**, 1049-1056.

[19] M Kanehisa, Y Sato, M Kawashima, M Furumichi and M Tanabe. KEGG as a reference resource for gene and protein annotation. *Nucleic Acids Research* 2016; **44(1)**, 457-462.

[20] TH Ngau. Assessment of phytochemical composition, antimicrobial, antioxidant activities, and cytotoxicity of the ethanol extract from Cordyceps militaris. *Journal of Science Technology and Food* 2022; **22(3)**, 13-23.

[21] TT Le, HT Duong and CH Nguyen. Characterization of *in vitro* antimicrobial activity of gyrophoric acid isolated from *Parmotrema indicum* on methicillin-resistant *Staphylococcus aureus*. *Journal of Applied Pharmaceutical Science* 2024; **14(3)**, 45-54.

[22] TH Ngau, TTB Ngoc, LTY Nhi, NH Chuong and DTP Thao. Anticancer property of marine coral-derived *Streptomyces sp*. SS162 against A549 lung adenocarcinoma cancer cells. *Journal of Applied Pharmaceutical Science* 2023; **13(10)**, 188-198.

[23] VTK Tran, TT Le, CH Nguyen, TNT Tran and V Hoang. Chemical composition, antibacterial, anticancer, and anti-a-glucosidase activities of essential oils from *Alpinia nelumboides*. *Journal of Applied Pharmaceutical Science* 2024; **14(12)**, 68-75.

[24] B Buranrat. Cratoxylum formosum leaf extracts inhibit growth, induce apoptosis, and decrease metastasis of hela human cervical cancer cells. *Pharmacognosy Magazine* 2022; **18(78)**, 296-303.

[25] X Bai, J Wang, L Zhang, J Ma, H Zhang, S Xia, M Zhang, X Ma, Y Guo, R Rong, S Cheng, W Shu, Y Wang and J Leng. Prostaglandin E_2 receptor EP1-mediated phosphorylation of focal adhesion kinase enhances cell adhesion and migration in hepatocellular carcinoma cells. *International Journal of Oncology* 2013; **42(5)**, 1833-1841.

[26] H Assaggaf, NE Hachlafi, ME fadili, A Elbouzidi, H Ouassou, M Jeddi, S Alnasser, A Qasem, A Attar, A Al-Farga, OA Alghamdi, EE Mehana and HN Mrabti. GC/MS Profiling, *In vitro* antidiabetic efficacy of origanum compactum benth. essential oil and *in silico* molecular docking of its major bioactive compounds. *Catalysts* 2023; **13(11)**, 1429.

[27] TD Nguyen,CDM Huynh,TT Le, PNT Dao, HTT Nguyen, THT Vo, NH Phan, BT Ngo-Huynh and V Hoang. Chemical composition and antifungal activities of *Vitex rotundifolia* essential oil from Vietnam: *In vitro* and *in silico* study. *Journal of Essential Oil-Bearing Plants* 2025; **28(6)**, 1369-1380.

[28] W Guo, H Wang and C Li. Signal pathways of melanoma and targeted therapy. *Signal Transduction and Targeted Therapy* 2021; **6**, 424.

[29] Y Liu, X Yang, J Gan, S Chen, ZX Xiao and Y Cao. CB-Dock2: Improved protein-ligand blind docking by integrating cavity detection, docking and homologous template fitting. *Nucleic Acids Research* 2022; **50(1)**, 159-164.

[30] A Daina, O Michielin and V Zoete. SwissADME: A free web tool to evaluate pharmacokinetics, drug-likeness and medicinal chemistry friendliness of small molecules. *Scientific Reports* 2017; **7**, 42717.

[31] CA Lipinski. Lead- and drug-like compounds: The rule-of-five revolution. *Drug Discovery Today: Technologies* 2004; **1(4)**, 337-341.

[32] A Daina, O Michielin and V Zoete. SwissTargetPrediction: Updated data and new features for efficient prediction of protein targets of small molecules. *Nucleic Acids Research* 2019; **47(1)**, 357-364.

[33] M Liao, JJ Xiao, LJ Zhou, Y Liu, XW Wu, RM Hua, GR Wang and HQ Cao. Insecticidal activity of melaleuca alternifolia essential oil and RNA-Seq analysis of *Sitophilus zeamais* transcriptome in response to oil fumigation. *PLoS One* 2016; **11(12)**, 0167748.

[34] SX Ge and D Jung. ShinyGO: A web application for in-depth analysis of gene sets. *Bioinformatics* 2020; **36(8)**, 2628-2629.

[35] Kaplan-Meier Plotter, Available at: http://www.kmplot.com/analysis, accessed December 2025.

[36] V Kuete, O Karaosmanoğlu and H Sivas. *Chapter 10 - anticancer activities of African medicinal spices and vegetables*. RELX, London, 2017, p. 271-297.

[37] S Sangthong, I Promputtha, P Pintathong and P Chaiwut. Chemical constituents, antioxidant, anti-tyrosinase, cytotoxicity, and anti-melanogenesis activities of *Etlingera elatior* (Jack) leaf essential oils. *Molecules* 2022; **27(11)**, 3469.

[38] PF de Oliveira, JM Alves, JL Damasceno, RAM Oliveira, HJ Dias, AEM Crotti and DC Tavares. Cytotoxicity screening of essential oils in cancer cell lines. *Revista Brasileira de Farmacognosia* 2015; **25(2)**, 183-188.

[39] M Sharma, K Grewal, R Jandrotia, DR Batish, HP Singh and RK Kohli. Essential oils as anticancer agents: Potential role in malignancies, drug delivery mechanisms, and immune system enhancement. *Biomedicine & Pharmacotherapy* 2022; **146**, 112514.

[40] TA Pham, IS Mohammad, VT Vu, XL Hu, C Birendra, A Ulah, C Guo, XY Lü, WC Ye and H Wang. Phloroglucinol derivatives from the Fruits of *Eucalyptus globulus* and their cytotoxic activities. *Chemistry & Biodiversity* 2018; **15(6)**, 1800052.

[41] E Taheri, S Ghorbani, M Safi, NS Sani, FF Amoodizaj, M Heidari, R Chavoshi, S Hajazimian, A Isazadeh and M Heidari. Inhibition of colorectal cancer cell line CaCo-2 by essential oil of eucalyptus camaldulensis through induction of apoptosis. *Acta Medica Iranica* 2020: **58(6)**, 260-265.

[42] A Joshi, A Sharma, RK Bachheti and DP Pandey. A comparative study of the chemical composition of the essential oil from *Eucalyptus globulus* growing in dehradun (India) and around the World. *Oriental Journal of Chemistry* 2016; **32(1)**, 331-340.

[43] MD Martile, S Garzoli, R Ragno and DD Bufalo. Essential oils and their main chemical components: The Past 20 Years of preclinical studies in melanoma. *Cancers* 2020; **12**, 2650.

[44] CH Yang, YC Huang, ML Tsai, CY Cheng, LL Liu, YW Yen and WL Chen. Inhibition of melanogenesis by β-caryophyllene from lime mint essential oil in mouse B16 melanoma cells. *International Journal of Cosmetic Science* 2015; **37(5)**, 550-554.

[45] KJS Kumar, MG Vani, PC Wu, HJ Lee, YH Tseng and SY Wang. Essential oils of *Alpinia nantoensis* retard forskolin-induced melanogenesis via ERK1/2-Mediated proteasomal degradation of MITF. *Plants* 2020; **9(12)**, 1672.

[46] K Sebei, F Sakouhi, W Herchi, ML Khouja and S Boukhchina. Chemical composition and antibacterial activities of seven *Eucalyptus species* essential oils leaves. *Biological Research* 2015; **48**, 7.

[47] M Burotto, VL Chiou, JM Lee and EC Kohn. The MAPK pathway across different malignancies: A new perspective. *Cancer* 2014; **120(22)**, 3446-3456.

[48] R Acharya, S Chacko, P Bose, A Lapenna and SP Pattanayak. Structure based multitargeted molecular docking analysis of selected furanocoumarins against breast cancer. *Scientific Reports* 2019; **9**, 15743.

[49] D Ramachandhiran, C Sankaranarayanan, R Murali, S Babukumar and V Vinothkumar. β-Caryophyllene promotes oxidative stress and apoptosis in KB cells through activation of mitochondrial-mediated pathway: An *in-vitro* and

in-silico study. *Archives of Physiology and Biochemistry* 2022; **128**, 148-162.

[50] F Mannino, G Pallio, R Corsaro, L Minutoli, D Altavilla, G Vermiglio, A Allegra, AH Eid, A Bitto, F Squadrito and N Irrera. Beta-caryophyllene exhibits anti-proliferative effects through apoptosis induction and cell cycle modulation in multiple myeloma cells. *Cancers* 2021; **13(22)**, 5741.

[51] MT Mahanthesh, D Ranjith, R Yaligar, R Jyothi, G Narappa and MV Ravi. Swiss ADME prediction of phytochemicals present in *Butea monosperma* (Lam.) Taub. *Journal of Pharmacognosy and Phytochemistry* 2020, **9(3)**, 1799-1809.

[52] TT Le, TD Nguyen, MT Nguyen-Van, TNB Huynh, TT Dinh, CDM Huynh, PDT Nguyen, TNV Ho, H Tran-Van and V Hoang. Antifungal mechanisms of *Melaleuca bracteata* F. Mueall essential oil against Candida albicans: From chemical profiling to molecular targets. *European Journal of Integrative Medicine* 2025; **80**, 102570.

[53] RW Dellinger, HH Matundan, AS Ahmed, PH Duong and FLM Jr. Anti-cancer drugs elicit re-expression of UDP-Glucuronosyltransferases in melanoma cells. *PLoS One* 2012; **7(10)**, 47696.

[54] Y Yamauchi, K Furukawa, K Hamamura and K Furukawa. Positive feedback loop between PI3K-Akt-mTORC1 signaling and the lipogenic pathway boosts Akt signaling: Induction of the lipogenic pathway by a melanoma antigen. *Cancer Research* 2011; **71(14)**, 4989-4997.

[55] A Yamazaki, I Omura, Y Kamikawa, M Hide, A Tanaka, M Kaneko, K Imaizumi and A Saito. Unfolded protein response modulates Tyrosinase levels and melanin production during melanogenesis. *Journal of Dermatological Science* 2025; **117(2)**, 36-44.

Supplementary Material

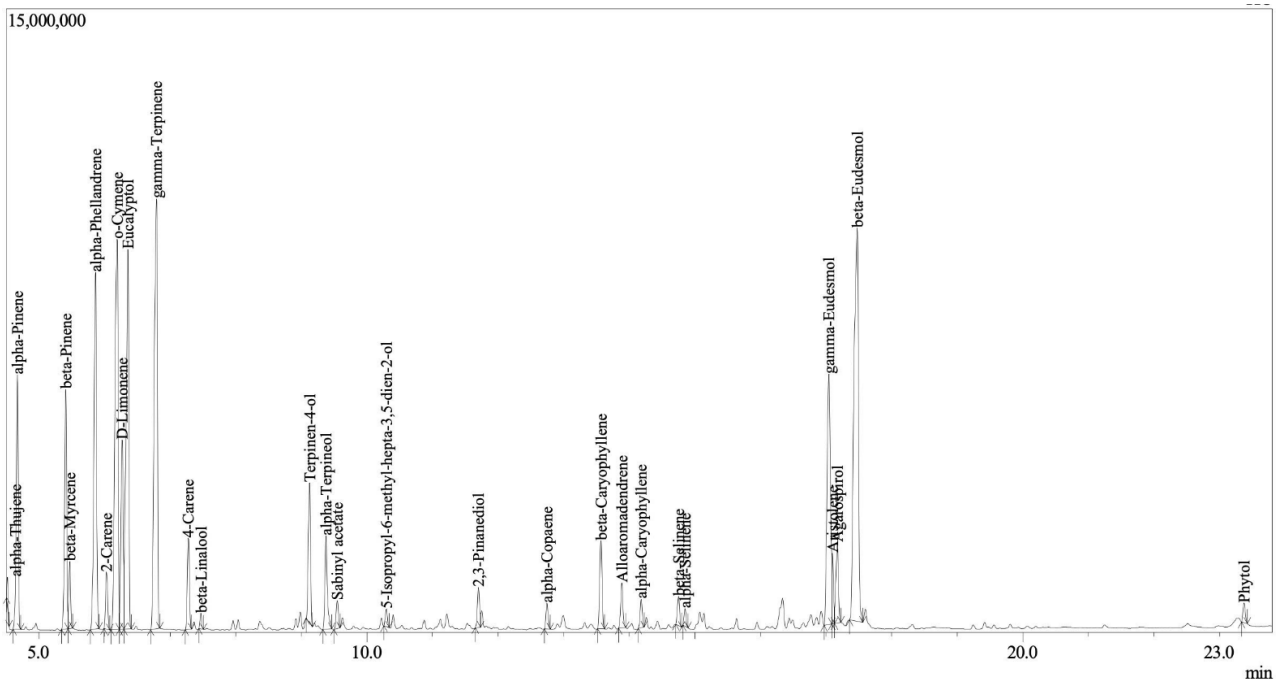

Figure S1 Gas chromatography analysis of *E. camaldulensis* essential oils.

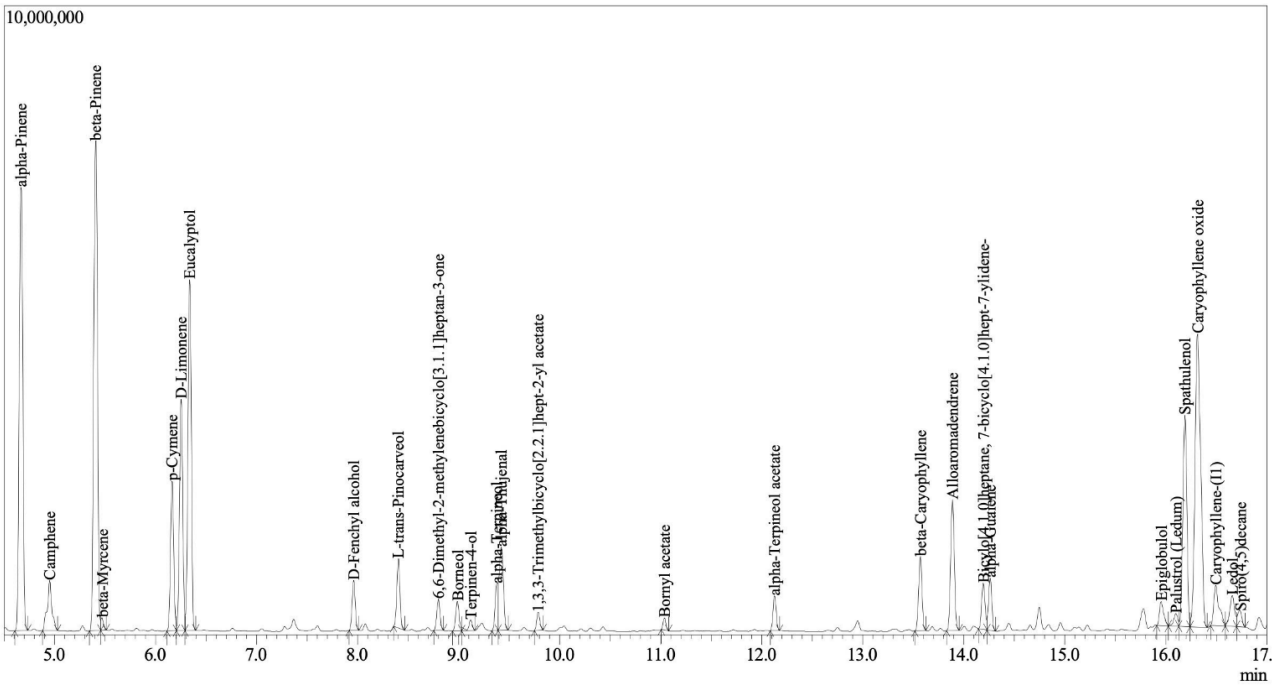

Figure S2 Gas chromatography analysis of *E. tereticornis* essential oils.

Table S1 Docking results of Top-Ranked potential drugs compound with target protein by CB-Dock2.

No	Code	Protein	Cid	Compound	Gravity	Energy
1	6XFP	BRAF	562714	Bicylo[4.1.0]heptane,7 bicyclo[4.1.0]hept-7-ylidene	1	-8.5
2	1MP8	FAK	10899740	Alloaromadendrene	1	-8.2
3	6XFP	BRAF	19725	alpha-Copaene	2	-8.2
4	6XFP	BRAF	110745	Palustrol (Ledum)	1	-8.2
5	6XFP	BRAF	5369754	Caryophyllene-(l1)	2	-8.2
6	6XFP	BRAF	5281520	alpha-Caryophyllene	1	-8.1
7	6XFP	BRAF	10899740	Alloaromadendrene	2	-8.1
8	6XFP	BRAF	91457	**beta-Eudesmol**	2	-7.9
9	6XFP	BRAF	92812	Ledol	2	-7.9
10	6XFP	BRAF	5280435	Phytol	1	-7.9
11	6XFP	BRAF	5317844	alpha-Guaiene	1	-7.9
12	6XFP	BRAF	6432005	gamma-Eudesmol	1	-7.9
13	6XFP	BRAF	11858788	Epiglobulol	2	-7.9
14	6XFP	BRAF	21675005	Agarospirol	1	-7.9
15	6XFP	BRAF	5281515	beta-Caryophyllene	2	-7.8
16	8VM2	NRAS	5369754	Caryophyllene-(l1)	1	-7.8
17	1MP8	FAK	92231	**Spathulenol**	1	-7.7
18	1MP8	FAK	110745	Palustrol (Ledum)	1	-7.7
19	6XFP	BRAF	442393	beta-Selinene	1	-7.7
20	8VM2	NRAS	92231	**Spathulenol**	1	-7.7
21	6XFP	BRAF	10856614	alpha-Selinene	1	-7.6
22	1MP8	FAK	5281515	beta-Caryophyllene	1	-7.5
23	1MP8	FAK	5281520	alpha-Caryophyllene	1	-7.5
24	1MP8	FAK	10856614	alpha-Selinene	1	-7.5
25	6XFP	BRAF	92231	**Spathulenol**	1	-7.5
26	6XFP	BRAF	1742210	**Caryophyllene oxide**	2	-7.5
27	1MP8	FAK	92812	Ledol	1	-7.4
28	1MP8	FAK	562714	Bicylo[4.1.0]heptane,7 bicyclo[4.1.0]hept-7-ylidene	1	-7.4
29	6XFP	BRAF	9585226	6,6-Dimethyl-2 methylenebicyclo[3.1.1]heptan-3-one	1	-7.4
30	8VM2	NRAS	6432005	gamma-Eudesmol	1	-7.4
31	1MP8	FAK	442393	beta-Selinene	1	-7.3
32	1MP8	FAK	1742210	**Caryophyllene oxide**	1	-7.3
33	1MP8	FAK	5317844	alpha-Guaiene	1	-7.3
34	1MP8	FAK	19725	alpha-Copaene	1	-7.2
35	1MP8	FAK	5369754	Caryophyllene-(l1)	1	-7.2
36	6XFP	BRAF	111037	alpha-Terpineol acetate	1	-7.2
37	6XFP	BRAF	530421	Aristolene	2	-7.2
38	1MP8	FAK	6432005	gamma-Eudesmol	1	-7.1

No	Code	Protein	Cid	Compound	Gravity	Energy
39	1MP8	FAK	11858788	Epiglobulol	1	-7.1
40	8VM2	NRAS	442393	beta-Selinene	1	-7.1
41	8VM2	NRAS	10856614	alpha-Selinene	1	-7.1
42	1MP8	FAK	91457	**beta-Eudesmol**	1	-6.9
43	6XFP	BRAF	1201530	L-trans-Pinocarveol	2	-6.9
44	8VM2	NRAS	5280435	Phytol	1	-6.9
45	8VM2	NRAS	5363138	5-Isopropyl-6-methyl-hepta-3,5-dien 2-ol	1	-6.9
46	8VM2	NRAS	10899740	Alloaromadendrene	1	-6.9
47	6XFP	BRAF	94266	Sabinyl acetate	2	-6.8
48	6XFP	BRAF	107217	1,3,3-Trimethylbicyclo[2.2.1]hept-2-yl acetate	2	-6.8
49	6XFP	BRAF	5363138	5-Isopropyl-6-methyl-hepta-3,5-dien 2-ol	2	-6.8
50	8VM2	NRAS	91457	**beta-Eudesmol**	1	-6.8
51	8VM2	NRAS	110745	Palustrol (Ledum)	1	-6.8
52	8VM2	NRAS	5281515	beta-Caryophyllene	1	-6.8
53	8VM2	NRAS	5281520	alpha-Caryophyllene	1	-6.8
54	8VM2	NRAS	21675005	Agarospirol	1	-6.8
55	1MP8	FAK	530421	Aristolene	1	-6.7
56	1MP8	FAK	21675005	Agarospirol	1	-6.7
57	6XFP	BRAF	17868	alpha-Thujene	2	-6.7
58	8VM2	NRAS	5317844	alpha-Guaiene	1	-6.7
59	6XFP	BRAF	6448	Bornyl acetate	2	-6.6
60	6XFP	BRAF	7460	**alpha-Phellandrene**	1	-6.6
61	8VM2	NRAS	111037	alpha-Terpineol acetate	1	-6.6
62	6XFP	BRAF	17100	alpha-Terpineol	2	-6.5
63	8VM2	NRAS	92812	Ledol	1	-6.5
64	6XFP	BRAF	7461	**gamma-Terpinene**	2	-6.4
65	6XFP	BRAF	11230	Terpinen-4-ol	2	-6.4
66	6XFP	BRAF	440917	D-Limonene	2	-6.4
67	6XFP	BRAF	440967	**beta-Pinene**	2	-6.4
68	8VM2	NRAS	19725	alpha-Copaene	1	-6.4
69	8VM2	NRAS	562714	Bicylo[4.1.0]heptane,7 bicyclo[4.1.0]hept-7-ylidene	1	-6.4
70	8VM2	NRAS	1742210	**Caryophyllene oxide**	1	-6.4
71	8VM2	NRAS	11858788	Epiglobulol	1	-6.4
72	2X18	AKT3	92812	Ledol	4	-6.3
73	6XFP	BRAF	6654	**alpha-Pinene**	2	-6.3
74	6XFP	BRAF	7463	p-Cymene	2	-6.3
75	6XFP	BRAF	10703	**o-Cymene**	2	-6.3
76	6XFP	BRAF	62044	2,3-Pinanediol	1	-6.3

No	Code	Protein	Cid	Compound	Gravity	Energy
77	6XFP	BRAF	79044	2-Carene	1	-6.3
78	8VM2	NRAS	94266	Sabinyl acetate	1	-6.3
79	1MP8	FAK	5363138	5-Isopropyl-6-methyl-hepta-3,5-dien 2-ol	1	-6.2
80	6WHO	HDC	6432005	gamma-Eudesmol	2	-6.2
81	6XFP	BRAF	530422	4-Carene	1	-6.2
82	8VM2	NRAS	10703	**o-Cymene**	1	-6.2
83	1MP8	FAK	94266	Sabinyl acetate	1	-6.1
84	1MP8	FAK	111037	alpha-Terpineol acetate	1	-6.1
85	6XFP	BRAF	2758	**Eucalyptol**	1	-6.1
86	1MP8	FAK	107217	1,3,3-Trimethylbicyclo[2.2.1]hept-2-yl acetate	3	-6
87	2X18	AKT3	6432005	gamma-Eudesmol	2	-6
88	6XFP	BRAF	135982	Spiro(4,5)decane	1	-6
89	8VM2	NRAS	7461	**gamma-Terpinene**	1	-6
90	8VM2	NRAS	7463	p-Cymene	1	-6

Table S2 Gene sets were used in GO – KEGG and survival analysis.

Compounds	Gene					
	Bicylo[4.1.0]heptane,7 bicyclo[4.1.0]hept-7-ylidene	**Alloaromadendrene**	**α-Copaene**	**Palustrol (Ledum)**	**Caryophyllene-(l1)**	**alpha-Caryophyllene**
1	*FAAH*	*NR1H3*	*ESR1*	*UGT2B7*	*SQLE*	*SQLE*
2	*TRPV1*	*NR1H2*	*CHRM2*	*UGT2B11*	*FAAH*	*GLI1*
3	*TRPV4*	*UGT2B7*	*AR*	*UGT2B17*	*TRPV1*	*GLI2*
4	*TRPV2*	*UGT2B11*	*CYP19A1*	*UGT2B4*	*TRPV4*	*GLI3*
5	*SQLE*	*UGT2B17*	*ACHE*	*UGT2B10*	*TRPV2*	*TRPV1*
6	*UGT2B7*	*UGT2B4*	*SLC6A2*	*UGT2B15*	*NR1H2*	*TRPV4*
7	*UGT2B11*	*UGT2B10*	*SLC6A4*	*UGT2A3*	*NR1H3*	*TRPV2*
8	*UGT2B17*	*UGT2B15*	*CYP2C19*	*UGT2B28*	*TOP1*	*CNR1*
9	*UGT2B4*	*UGT2A3*	*SLC6A3*	*UGT2A1*	*Q969P6*	*PPARG*
10	*UGT2B10*	*UGT2B28*	*ESR2*	*ESR1*	*ESR1*	*PPARD*
11	*UGT2B15*	*UGT2A1*	*CHRM4*	*AR*	*CHRM2*	*PPARA*
12	*UGT2A3*	*LDLR*	*CHRM5*	*UGT1A4*	*AR*	*ALOX5*
13	*UGT2B28*	*VLDLR*	*CHRM1*	*CDC25A*	*CYP19A1*	*ALOX15B*
14	*UGT2A1*	*LRP8*	*CHRM3*	*CDC25B*	*ACHE*	*O75342*
15	*ESR1*	*TDP1*	*BCHE*	*ESR2*	*SLC6A2*	*ALOX15*
16	*BRAF*	*BRAF*	*BRAF*	*BRAF*	*BRAF*	*BRAF*
17	*NRAS*	*NRAS*	*NRAS*	*NRAS*	*NRAS*	*NRAS*
18	*AKT3*	*AKT3*	*AKT3*	*AKT3*	*AKT3*	*AKT3*
19	*FAK*	*FAK*	*FAK*	*FAK*	*FAK*	*FAK*
20	*HDAC2*	*HDAC2*	*HDAC2*	*HDAC2*	*HDAC2*	*HDAC2*

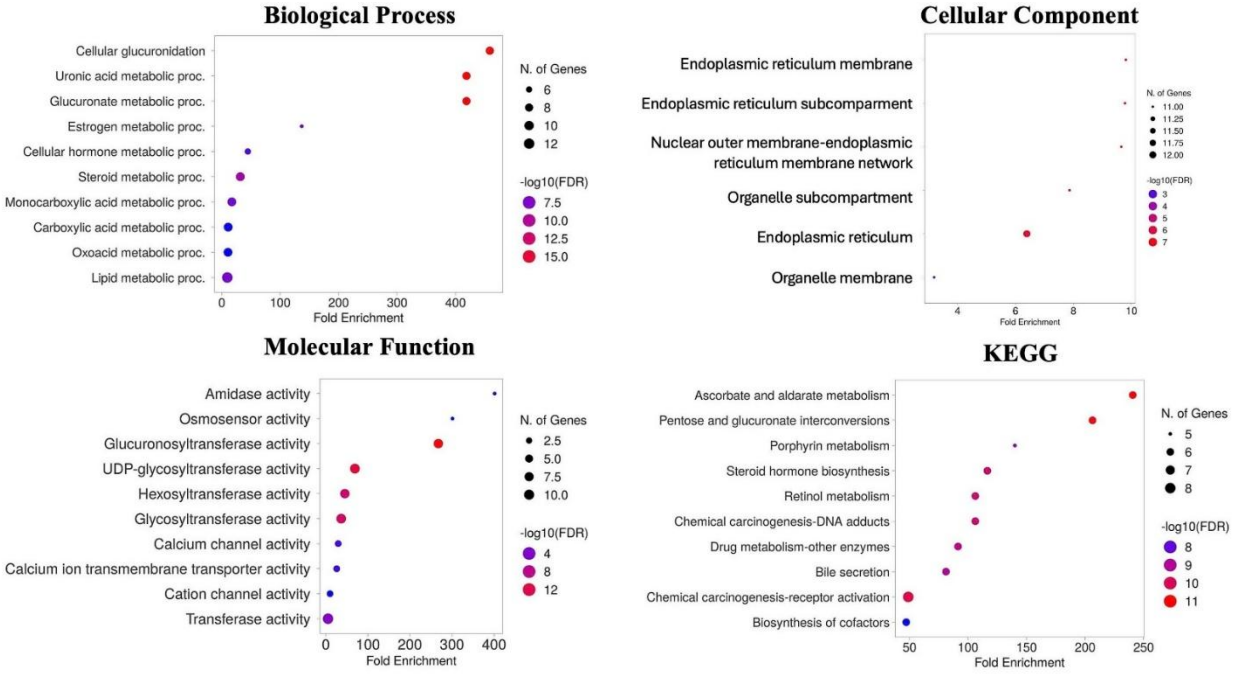
Biological Process
Cellular glucuronidation
Uronic acid metabolic proc.
Glucuronate metabolic proc.
Estrogen metabolic proc.
Cellular hormone metabolic proc.
Steroid metabolic proc.
Monocarboxylic acid metabolic proc.
Carboxylic acid metabolic proc.
Oxoacid metabolic proc.
Lipid metabolic proc.
0 100 200 300 400
Fold Enrichment
N. of Genes
6
8
10
12
-log10(FDR)
7.5
10.0
12.5
15.0
Cellular Component
Endoplasmic reticulum membrane
Endoplasmic reticulum subcomparment
Nuclear outer membrane-endoplasmic reticulum membrane network
Organelle subcompartment
Endoplasmic reticulum
Organelle membrane
4 6 8 10
Fold Enrichment
N. of Genes
11.00
11.25
11.50
11.75
12.00
-log10(FDR)
3
4
5
6
7
Molecular Function
Amidase activity
Osmosensor activity
Glucuronosyltransferase activity
UDP-glycosyltransferase activity
Hexosyltransferase activity
Glycosyltransferase activity
Calcium channel activity
Calcium ion transmembrane transporter activity
Cation channel activity
Transferase activity
0 100 200 300 400
Fold Enrichment
N. of Genes
2.5
5.0
7.5
10.0
-log10(FDR)
4
8
12
KEGG
Ascorbate and aldarate metabolism
Pentose and glucuronate interconversions
Porphyrin metabolism
Steroid hormone biosynthesis
Retinol metabolism
Chemical carcinogenesis-DNA adducts
Drug metabolism-other enzymes
Bile secretion
Chemical carcinogenesis-receptor activation
Biosynthesis of cofactors
50 100 150 200 250
Fold Enrichment
N. of Genes
5
6
7
8
-log10(FDR)
8
9
10
11

(A)

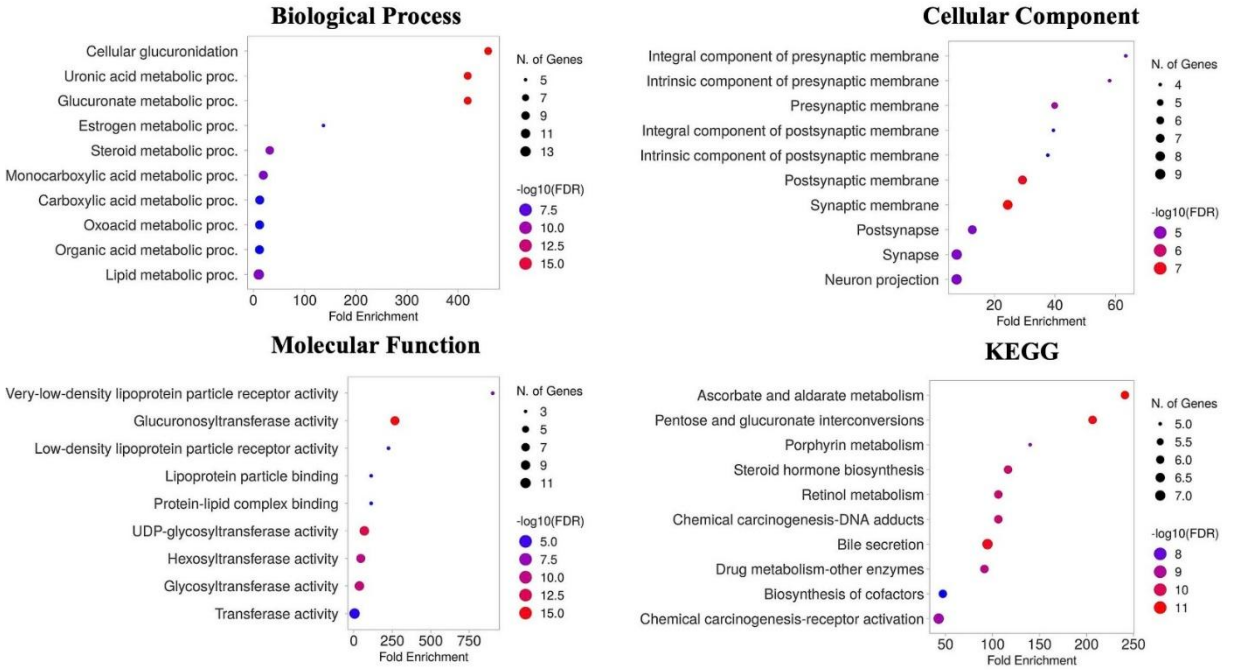
Biological Process
Cellular glucuronidation
Uronic acid metabolic proc.
Glucuronate metabolic proc.
Estrogen metabolic proc.
Steroid metabolic proc.
Monocarboxylic acid metabolic proc.
Carboxylic acid metabolic proc.
Oxoacid metabolic proc.
Organic acid metabolic proc.
Lipid metabolic proc.
0 100 200 300 400
Fold Enrichment
N. of Genes
5
7
9
11
13
-log10(FDR)
7.5
10.0
12.5
15.0
Cellular Component
Integral component of presynaptic membrane
Intrinsic component of presynaptic membrane
Presynaptic membrane
Integral component of postsynaptic membrane
Intrinsic component of postsynaptic membrane
Postsynaptic membrane
Synaptic membrane
Postsynapse
Synapse
Neuron projection
20 40 60
Fold Enrichment
N. of Genes
4
5
6
7
8
9
-log10(FDR)
5
6
7
Molecular Function
Very-low-density lipoprotein particle receptor activity
Glucuronosyltransferase activity
Low-density lipoprotein particle receptor activity
Lipoprotein particle binding
Protein-lipid complex binding
UDP-glycosyltransferase activity
Hexosyltransferase activity
Glycosyltransferase activity
Transferase activity
0 250 500 750
Fold Enrichment
N. of Genes
3
5
7
9
11
-log10(FDR)
5.0
7.5
10.0
12.5
15.0
KEGG
Ascorbate and aldarate metabolism
Pentose and glucuronate interconversions
Porphyrin metabolism
Steroid hormone biosynthesis
Retinol metabolism
Chemical carcinogenesis-DNA adducts
Bile secretion
Drug metabolism-other enzymes
Biosynthesis of cofactors
Chemical carcinogenesis-receptor activation
50 100 150 200 250
Fold Enrichment
N. of Genes
5.0
5.5
6.0
6.5
7.0
-log10(FDR)
8
9
10
11

(B)

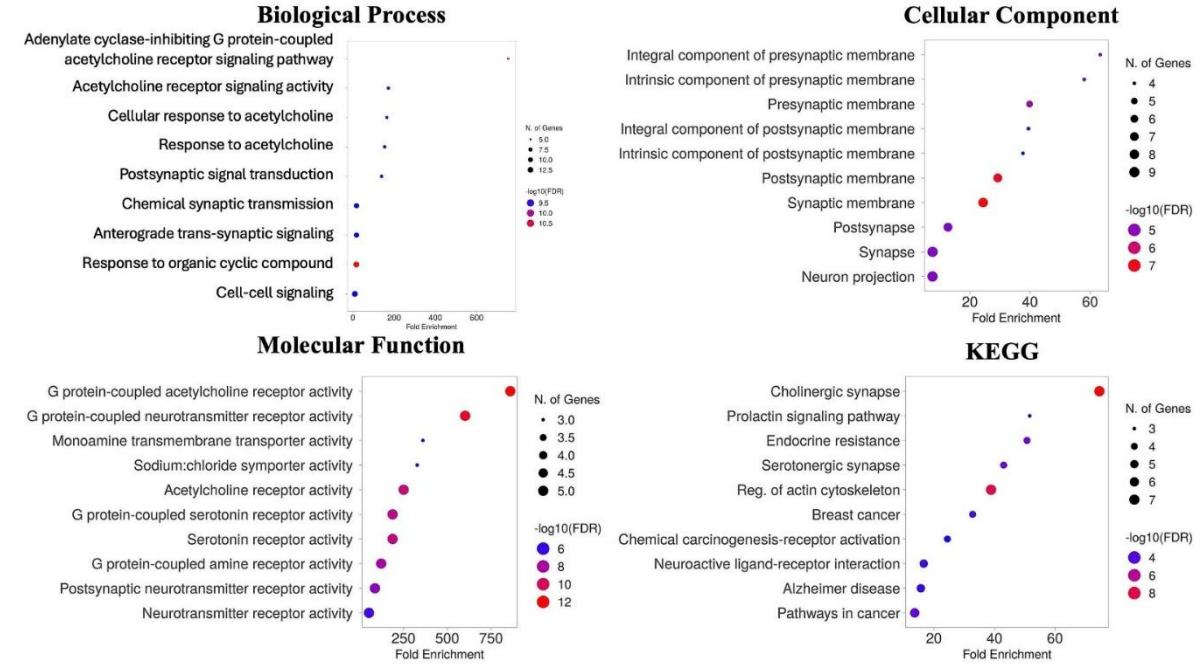
Biological Process
Adenylate cyclase-inhibiting G protein-coupled acetylcholine receptor signaling pathway
Acetylcholine receptor signaling activity
Cellular response to acetylcholine
Response to acetylcholine
Postsynaptic signal transduction
Chemical synaptic transmission
Anterograde trans-synaptic signaling
Response to organic cyclic compound
Cell-cell signaling
Fold Enrichment
Cellular Component
Integral component of presynaptic membrane
Intrinsic component of presynaptic membrane
Presynaptic membrane
Integral component of postsynaptic membrane
Intrinsic component of postsynaptic membrane
Postsynaptic membrane
Synaptic membrane
Postsynapse
Synapse
Neuron projection
Fold Enrichment
N. of Genes
-log10(FDR)
Molecular Function
G protein-coupled acetylcholine receptor activity
G protein-coupled neurotransmitter receptor activity
Monoamine transmembrane transporter activity
Sodium:chloride symporter activity
Acetylcholine receptor activity
G protein-coupled serotonin receptor activity
Serotonin receptor activity
G protein-coupled amine receptor activity
Postsynaptic neurotransmitter receptor activity
Neurotransmitter receptor activity
Fold Enrichment
KEGG
Cholinergic synapse
Prolactin signaling pathway
Endocrine resistance
Serotonergic synapse
Reg. of actin cytoskeleton
Breast cancer
Chemical carcinogenesis-receptor activation
Neuroactive ligand-receptor interaction
Alzheimer disease
Pathways in cancer
Fold Enrichment
N. of Genes
-log10(FDR)

(C)

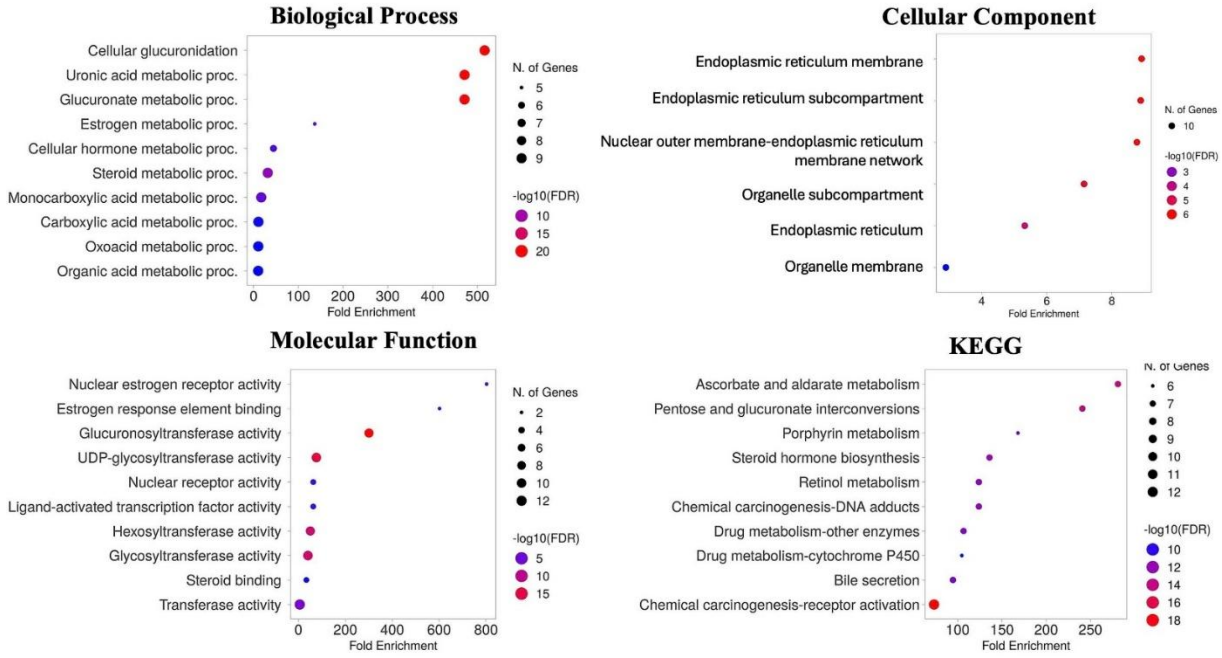
Biological Process
Cellular glucuronidation
Uronic acid metabolic proc.
Glucuronate metabolic proc.
Estrogen metabolic proc.
Cellular hormone metabolic proc.
Steroid metabolic proc.
Monocarboxylic acid metabolic proc.
Carboxylic acid metabolic proc.
Oxoacid metabolic proc.
Organic acid metabolic proc.
Fold Enrichment
Cellular Component
Endoplasmic reticulum membrane
Endoplasmic reticulum subcompartment
Nuclear outer membrane-endoplasmic reticulum membrane network
Organelle subcompartment
Endoplasmic reticulum
Organelle membrane
Fold Enrichment
N. of Genes
-log10(FDR)
Molecular Function
Nuclear estrogen receptor activity
Estrogen response element binding
Glucuronosyltransferase activity
UDP-glycosyltransferase activity
Nuclear receptor activity
Ligand-activated transcription factor activity
Hexosyltransferase activity
Glycosyltransferase activity
Steroid binding
Transferase activity
Fold Enrichment
KEGG
Ascorbate and aldarate metabolism
Pentose and glucuronate interconversions
Porphyrin metabolism
Steroid hormone biosynthesis
Retinol metabolism
Chemical carcinogenesis-DNA adducts
Drug metabolism-other enzymes
Drug metabolism-cytochrome P450
Bile secretion
Chemical carcinogenesis-receptor activation
Fold Enrichment
N. of Genes
-log10(FDR)

(D)

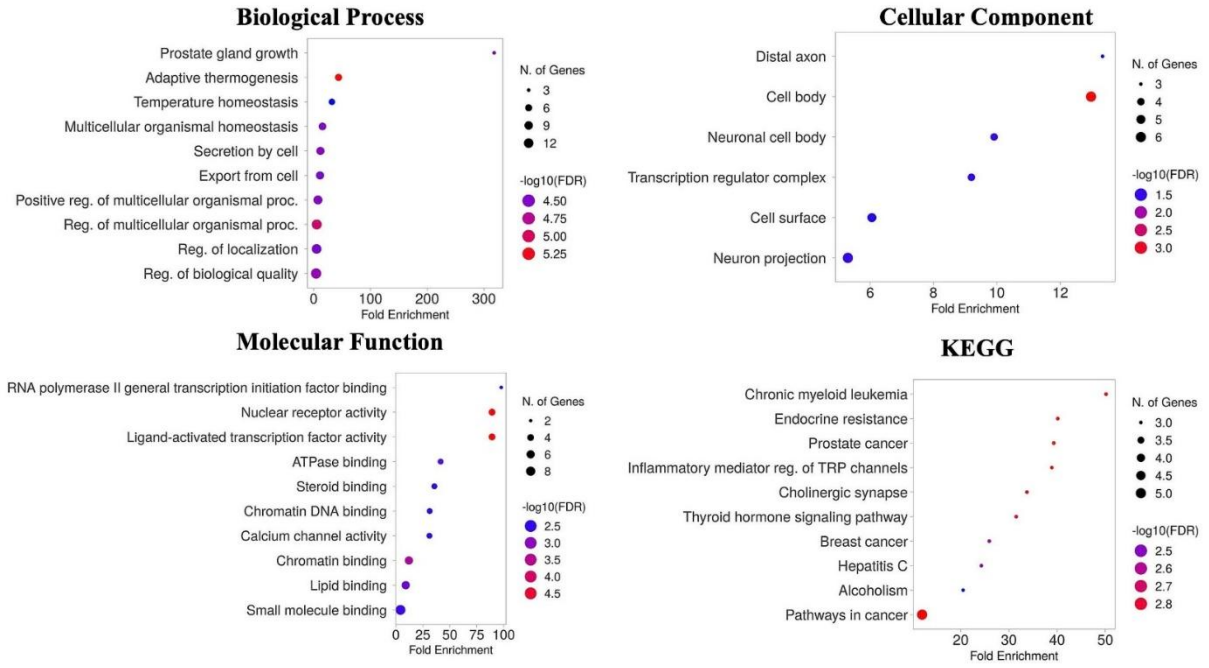

(E)

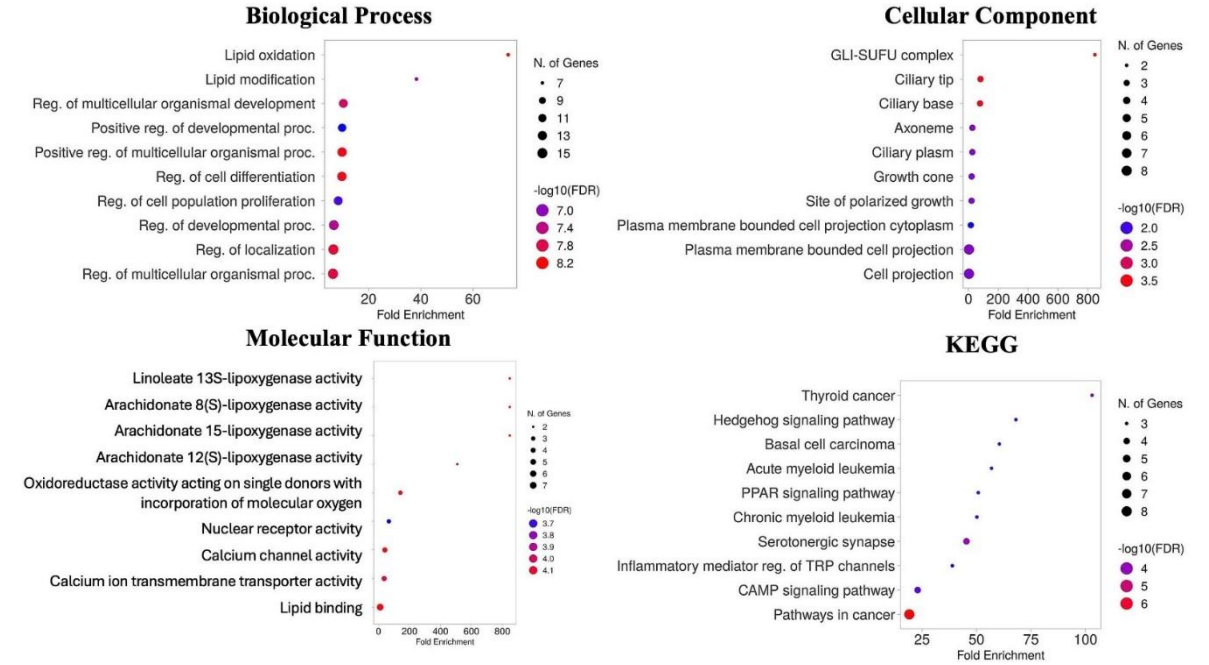

(F)

Figure S3 Pathway prediction including Biological processes, Cellular components, Molecular functions, KEGG pathways. (A) Bicylo[4.1.0]heptane,7 bicyclo[4.1.0]hept-7-ylidene; (B) Alloaromadendrene; (C) α-Copaene; (D) Palustrol (Ledum); (E) Caryophyllene-(l1); (F) α-Caryophyllene.

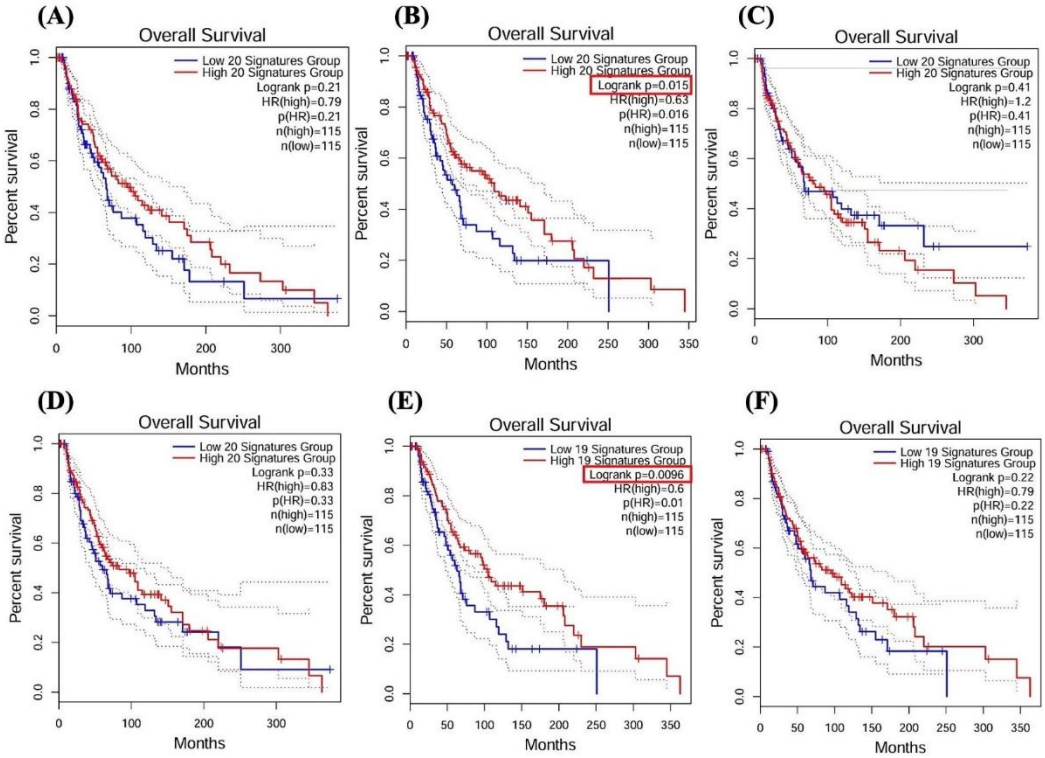

Figure S4 Kaplan-Meier survival analysis of compounds with skin cancer skin cutaneous melanoma (SKCM). (A) Bicylo[4.1.0]heptane,7 bicyclo[4.1.0]hept-7-ylidene; (B) Alloaromadendrene; (C) α-Copaene; (D) Palustrol (Ledum); (E) Caryophyllene-(l1); (F) α-Caryophyllene.